Chemical Physics Letters 490 (2010) 226–229

Contents lists available at ScienceDirect

Chemical Physics Letters

journal homepage: www.elsevier.com/locate/cplett

Regioselectivity on the cooxidation of 5,6-dihydroxyindole and its 2-carboxy derivative from the quantum chemical calculations

Hidekazu Okuda [a,*], Kazumasa Wakamatsu [b], Shosuke Ito [b], Takayuki Sota [a]

[a] Department of Electrical Engineering and Bioscience, Waseda University, Shinjuku, Tokyo 169-8555, Japan
[b] Department of Chemistry, Fujita Health University School of Health Sciences, Toyoake, Aichi 470-1192, Japan

ARTICLE INFO

Article history:
Received 6 October 2009
In final form 18 March 2010
Available online 20 March 2010

ABSTRACT

We report the heterodimerization of eumelanin precursors from the quantum chemical calculations using a general-purpose reactivity indicator. 5,6-Dihydroxyindole (DHI), its 2-carboxy derivative (DHICA), and related molecules are under consideration. Molecules participating in the reaction have been identified from the electron transfer probability. The heterodimerization has been demonstrated to be the electron-transfer-controlled reaction. The theoretical prediction is in good agreement with the result of the previous cooxidation of DHI and DHICA.

1. Introduction

Eumelanin is a brown-black macromolecular pigment and is a major component of human pigmentary system. 5,6-Dihydroxyindole (DHI, **1**) and its 2-carboxy derivative (DHICA, **2**) are key eumelanin building blocks [1–8]. The precise polymerization mechanism of them remains unclear. To attack the problem, many experimental efforts have been devoted to isolate oligomers of them [9–16].

Several homooligomers up to tetramers were isolated in the oxidation of **1** or **2** [9,10,12–16]. On the other hand, as for **1**–**2** heterooligomers, the only one oligomer, 5,5′,6,6′-tetrahydroxy-2′-carboxy-2,4′-biindolyl **3**, was isolated from the cooxidation of **1** and **2** [11]. The heteropolymerization mechanism is less understood than homopolymerization although eumelanin is considered to include the heteropolymer of **1** and **2** [1,3,5–8].

Theoretical studies have been already started in the field of eumelanin. **1**-related monomers [17,18], **2**-related monomers [19,20], and their oligomers have been studied [21–28]. The reactivity of **1**-related molecules was recently studied [27] to clarify the oxidative polymerization mechanism of **1** from the quantum chemical calculations using a general-purpose reactivity indicator [29,30]. The theoretical predictions from the quantum chemical calculation-based indicator reasonably explained the structural features of the isolated oligomers of **1**, and so the indicator may be considered useful also for studying the heteropolymerization of **1** and **2**.

In this Letter, we report the reactivity of the tautomers/conformers of **1**- and **2**-related molecules from theoretical point of view to clarify the heterodimerization mechanism of **1** and **2**. It is shown that the energies of the highest occupied molecular orbital (HOMO) and lowest unoccupied molecular orbital (LUMO) of each reactant molecule are associated remarkably with the heterodimerization mechanism: monoionic **1** and neutral **2**-quinone may participate in the heterodimerization, while most of **1** and **2** are considered to exist as neutral and monoionic forms, respectively, in near-neutral solution according to chemical insight.

2. Details of calculations

All quantum chemical calculations [31,32] have been carried out using the B3LYP hybrid functional [33], which consists of Becke's exchange functional and the slightly-modified Lee–Yang–Parr correlation functional. The 6-31++$G(d,p)$ basis set [34,35] has been used, which takes account of the d polarization functions on heavy atoms and p polarizations on hydrogen atoms and the diffuse functions for all atoms. The polarizable continuum model [36] has been used for taking the solvent effect into account. The effective point charge on each atom has been estimated by the CHelpG method [37]. Harmonic vibrational wavenumbers have been calculated analytically and scaled by 0.982. Excitation energies of molecules have been estimated using time-dependent density-functional theory (TD-DFT) [38] to evaluate the lowest excitation energy level, i.e., the energy of the LUMO. All quantum chemical calculations have been carried out using the GAUSSIAN03 program [39].

To estimate the reactivity of molecules, the general-purpose reactivity indicator [29,30] has been used. The indicator for nucleophiles is given by

$$\Xi^{\kappa}_{\Delta N\leqslant 0,\alpha} = (\kappa+1)q^{(0)}_{\alpha} - \Delta N(\kappa-1)\left[q^{(-)}_{\alpha} - q^{(0)}_{\alpha}\right] = (\kappa+1)q^{(0)}_{\alpha} - \Delta N(\kappa-1)f^{-}_{\alpha}, \quad (1)$$

* Corresponding author. Fax: +81 3 3207 1488.
E-mail address: h.okuda@aoni.waseda.jp (H. Okuda).

0009-2614/$ - see front matter © 2010 Elsevier B.V. All rights reserved.
doi:10.1016/j.cplett.2010.03.054

and that for electrophiles is given by

$$\Xi^{\kappa}_{\Delta N\geqslant 0,\alpha} = -(\kappa+1)q^{(0)}_{\alpha} + \Delta N(\kappa-1)\left[q^{(0)}_{\alpha} - q^{(-)}_{\alpha}\right] = -(\kappa+1)q^{(0)}_{\alpha} + \Delta N(\kappa-1)f^{-}_{\alpha}. \quad (2)$$

Here, subscript α specifies the reactive position; $q^{(0)}_{\alpha}$ means the effective point charge on α; $q^{(-)}_{\alpha}$ and $q^{(+)}_{\alpha}$ denote the effective point charge on α for the radical cation of the nucleophile without a transferring electron and that for the radical anion of the electrophile with an additional electron, respectively; $f^{\pm}_{\alpha}$ denotes the condensed Fukui functions on α defined as $f^{\pm}_{\alpha} = \pm q^{(0)}_{\alpha} \mp q^{(\pm)}_{\alpha}$. The two parameters, ΔN and κ, are also included. ΔN denotes the amount of electron transfer in the reaction. By varying the value κ, the indicator covers the entire chemical reactions: strong electrostatic control ($\kappa > 1$), pure electrostatic control ($\kappa = 1$), joint control by electrostatics and electron-transfer effects ($-1 < \kappa < 1$), pure electron-transfer control ($\kappa = -1$), strong electron-transfer control ($\kappa < -1$). The most reactive position of the molecule is the reactive position with the most negative $\Xi^{\kappa}_{\Delta N,\alpha}$. Note that the reactive indices should be estimated with including the adjacent hydrogen atom [29].

In this Letter, the probability of finding each tautomer/conformer has been estimated from the Boltzmann factor (f_B), which depends exponentially on both relative energy and temperature:

$$f_{B,i} = \exp\left(-\frac{\Delta G_i}{k_B T}\right), \quad (3)$$

where ΔG_i means difference of the free energy between the lowest energy molecule and the ith tautomer/conformer under consideration; k_B denotes Boltzmann constant; T is absolute temperature. The probability of finding the ith tautomer/conformer (P_i) is given as

$$P_i = \frac{f_{B,i}}{\sum_j f_{B,j}}. \quad (4)$$

In Eq. (4), j runs over all the tautomers/conformers. Throughout this Letter, T has been set to be 300 K.

As an index of possible reaction, the electron transfer probability between reactants in pH 7.0 has been estimated. The following is the procedure to estimate the electron transfer probability from a nucleophile, B, to an electrophile, A: The energy which an electron should overgo is

$$\Delta\varepsilon_{A,B} = \varepsilon_{LUMO,A} - \varepsilon_{HOMO,B}. \quad (5)$$

Here, ε_{LUMO} has been estimated from ε_{HOMO} and the excitation energy:

$$\varepsilon_{LUMO,i} = \varepsilon_{HOMO,i} + E^{ex}_i. \quad (6)$$

The probability of thermal excitation against $\Delta\varepsilon_{A,B}$ is

$$P^{ET}_{\Delta\varepsilon_{A,B}} = \exp\left(-\frac{\Delta\varepsilon_{A,B}}{k_B T}\right). \quad (7)$$

The electron transfer probability between molecules should include the probability of finding each molecule:

$$P^{ET}_{A,B} = P^{ET}_{\Delta\varepsilon_{A,B}} \times (P_A \times R_A) \times (P_B \times R_B), \quad (8)$$

where $P_A \times R_A$ and $P_B \times R_B$ denote the probability of finding A and B, respectively, including the difference between neutral forms and monoionic forms. P_A and P_B are estimated using the Eq. (4); R_A and R_B are estimated from pK_{an}:

$$R_A = \begin{cases} 1/(1+10^{4.25-7.0}) & \text{(A is a monoionic form)} \\ 10^{4.25-7.0}/(1+10^{4.25-7.0}) & \text{(A is a neutral form)} \end{cases}, \quad (9)$$

$$R_B = \begin{cases} 1/(1+10^{7.0-9.54}) & \text{(B is a neutral form)} \\ 10^{7.0-9.54}/(1+10^{7.0-9.54}) & \text{(B is a monoionic form)} \end{cases}. \quad (10)$$

Note that $pK_a = 4.25$, 9.76, 13.2 for **2**, $pK_a = 9.54$, 13.14 for **1** [40]. The probability of reactions occurring in units of % should be normalized:

$$P^{react}_{A,B} = \frac{P^{ET}_{A,B}}{\sum_{\alpha\in A}\sum_{\beta\in B} P^{ET}_{\alpha,\beta}} \times 100. \quad (11)$$

Here, α (β) runs over all electrophiles (nucleophiles).

3. Results and discussion

Molecular structures of **1N**, **1M**, **2N**, and **2M** (Fig. 1) were optimized in aqueous solution. Reasons why they are considered are explained below. The calculated values (bond length, bond angle, excitation energy) for the molecules were compared with the previous results for the related-molecules [17–19,41], validating the present calculations.

The **1**–**2** heterodimer (2,4′-biindolyl, **3**) was isolated in the cooxidation of **1** and **2** [11]. The increase in the yield of the formation of **3** with increasing **1**/**2** ratio suggested that **3** is formed via nucleophilic attacks of **1**-related molecules to **2**-quinones as electrophiles [11]. Therefore, only **1** (**2**)-related molecules were considered here as nucleophiles (electrophiles). It was shown from Hartree–Fock calculations for the monoanions of **2** [41] that the molecule dehydrogenated on the catecholic moiety is energetically preferred in ground state and may explain the absorption and emission spectra of **2**-solution. Thus, the molecules dehydrogenated on catecholic unit, such as **2Mc**, have been also under consideration although carboxylic acids are typically dissociated as $RCOO^-$ anions and H^+ cations in neutral solution. Note that the molecules which have no intramolecular hydrogen bond (open forms) are not considered because they are less stable [28]. Previous study demonstrates that ε_{HOMO} and ε_{LUMO} for each reactant molecule are significantly important to study the reaction picture [27], and thus, molecules such as **1M** or **2N** should be considered because the molecules have high ε_{HOMO} or low ε_{LUMO}.

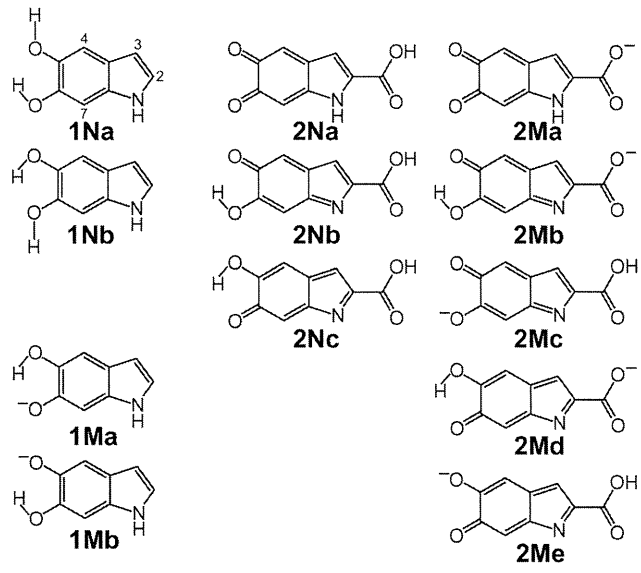

Fig. 1. Structural formula of **1N**, **1M**, **2N**, and **2M**. **1** and **2** act as nucleophiles and electrophiles, respectively. The atom-labeling usually used for indoles is also shown for **1Na**. **N** and **M** denote neutral and monoionic forms, respectively.

Table 1
Electron transfer probability ($P_{A,B}^{react}$) from a nucleophile to an electrophile in units of %.

	2Na	2Nb	2Nc	2Ma	2Mb	2Mc	2Md	2Me
1Na	$\sim 10^{-14}$	$\sim 10^{-16}$	$\sim 10^{-17}$	$\sim 10^{-16}$	$\sim 10^{-21}$	$\sim 10^{-27}$	$\sim 10^{-21}$	$\sim 10^{-27}$
1Nb	$\sim 10^{-15}$	$\sim 10^{-17}$	$\sim 10^{-17}$	$\sim 10^{-16}$	$\sim 10^{-22}$	$\sim 10^{-28}$	$\sim 10^{-22}$	$\sim 10^{-28}$
1Ma	94.06	1.19	0.37	4.08	$\sim 10^{-5}$	$\sim 10^{-12}$	$\sim 10^{-5}$	$\sim 10^{-12}$
1Mb	0.28	$\sim 10^{-3}$	$\sim 10^{-3}$	0.01	$\sim 10^{-8}$	$\sim 10^{-14}$	$\sim 10^{-8}$	$\sim 10^{-14}$

Since the polymerization of **1** is dominated by the electron-transfer-controlled reaction [27], the electron transfer probability from $\varepsilon_{HOMO,nucl}$ to $\varepsilon_{LUMO,elec}$ has been estimated in order to identify reactants. Results are summarized in Table 1 and suggest that the reaction of **1Ma** against **2Na** is plausible. The effective point charge, the condensed Fukui function, and the reactive indicator on each reactive position for **1Ma** and **2Na** are summarized in Table 2. Here the effective point charge for each reactive position includes that of its adjacent hydrogen atom [29]. Each reactive indicator has been calculated assuming $|\Delta N| = 1$ and $\kappa = -1$ as expected for the heteropolymerization.

In the previous study [27], we have proposed a method how regioselectivity is predicted from the effective point charge and general-purpose reactive indicator. Let us consider the reaction of **1Ma** against **2Na**. Judging from $\Xi^{\kappa=-1}_{|\Delta N|=1,\alpha}$, the C2 position is the most reactive for **1Ma**, while the C4 position is the most reactive for **2Na**. The effective point charge on the C2 position of **1Ma** is considered small enough not to prevent the formation of the C2–C4 bond between **1Ma** and **2Na**. Indeed, when the radical ion picture is used, the strongest Coulomb attraction acts between the C2 position of **1Ma** and the C4 position of **2Na**. Thus, 2,4′-biindolyl (**3**) may be formed via the reaction.

The present theory predicts **3** as a primary product of the cooxidation of **1** and **2** in accordance with the previous experimental result [11]. The formation scheme of **3** is shown in Fig. 2. The previous study [11] has reported one more heterooligomer in addition to **3**. However, to the best of our knowledge, its formula has not been experimentally identified, yet. Table 2 suggests that the unknown heterooligomer is 2,7′-biindolyl as a secondary product from the reaction of **1Ma** against **2Na**. Note that the reactivity of the C3 position of **2Na** is negligibly-small (Table 2). 2,7′-Biindolyl may be formed also via the reaction of **1Ma** against **2Ma**, the next plausible reaction (Table 1). It is because the C7 position is the most reactive position among the reactive positions of **2Ma** (not shown).

In this Letter, we have estimated the electron transfer probability using the lowest excitation energy within TD-DFT. This is validated from the two following reasons. First, TD-DFT is widely known to have enough accuracy for the excitation energy [42]. Indeed, the recent theoretical studies in the field of eumelanin have often used the method [17,22–26,28]. Second, the order of the electron transfer probability is important in this Letter. So the accuracy demanded about probability is not so high.

Table 2
Effective point charge, condensed Fukui function, and reactive indicator for each reactive position of **1Ma** and **2Na**. For the labels of the atoms, see Fig. 1.

		C2	C3	C4	C7
1Ma	$q_\alpha^{(0)}$	−0.0164	−0.1670	−0.2697	−0.3186
	$q_\alpha^{(-)}$	0.1760	0.1342	0.2223	0.1862
	f_α^-	0.1925	0.0328	0.0474	0.1324
	$\Xi^{\kappa=-1}_{\Delta N=-1,\alpha}$	0.3849	−0.0657	−0.0947	−0.2647
2Na	$q_\alpha^{(0)}$		−0.0746	−0.2110	−0.2369
	$q_\alpha^{(+)}$		−0.0899	−0.3296	−0.3104
	f_α^+		0.0152	0.1185	0.0735
	$\Xi^{\kappa=-1}_{\Delta N=1,\alpha}$		−0.0305	−0.2371	−0.1470

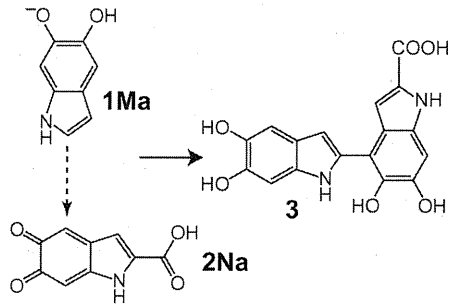

Fig. 2. Reaction scheme of formation of **3** from the theoretical prediction. The nucleophilic attack of the C2 position for **1Ma** to the C4 position for **2Na** leads to **3**.

In summary we have studied the cooxidation of DHI and DHICA from the quantum chemical calculations using the general-purpose reactive indicator. The theoretical prediction has agreed with the previous experimental results. The cooxidation of DHI and DHICA has been suggested to be the electron-transfer-controlled reaction. Which molecule participates in the reaction has been identified from the electron transfer probability.

References

[1] S. Ito, Pigment Cell Res. 16 (2003) 230.
[2] M. d'Ischia, A. Napolitano, A. Pezzella, E.J. Land, C.A. Ramsden, P.A. Riley, Adv. Heterocycl. Chem. 89 (2005) 1.
[3] P. Meredith, B.J. Powell, J. Riesz, S.P. Nighswander-Rempel, M.R. Pederson, E.G. Moore, Soft Matter 2 (2006) 37.
[4] P. Meredith, T. Sarna, Pigment Cell Res. 19 (2006) 572.
[5] S. Ito, K. Wakamatsu, Photochem. Photobiol. 84 (2008) 582.
[6] J.D. Simon, L. Hong, D.N. Peles, J. Phys. Chem. B 112 (2008) 13201.
[7] J.D. Simon, D. Peles, K. Wakamatsu, S. Ito, Pigment Cell Melanoma Res. 22 (2009) 563.
[8] M. d'Ischia, A. Napolitano, A. Pezzella, P. Meredith, T. Sarna, Angew. Chem. Int. Ed. 48 (2009) 3914.
[9] A. Napolitano, M.G. Corradini, G. Prota, Tetrahedron Lett. 26 (1985) 2805.
[10] M. d'Ischia, A. Napolitano, K. Tsiakas, G. Prota, Tetrahedron 46 (1990) 5789.
[11] A. Napolitano, O. Crescenzi, G. Prota, Tetrahedron Lett. 34 (1993) 885.
[12] A. Pezzella, A. Napolitano, M. d'Ischia, G. Prota, Tetrahedron 52 (1996) 7913.
[13] A. Pezzella, D. Vogna, G. Prota, Tetrahedron 58 (2002) 3681.
[14] A. Pezzella, D. Vogna, G. Prota, Tetrahedron: Asymmetry 14 (2003) 1133.
[15] L. Panzella, A. Pezzella, A. Napolitano, M. d'Ischia, Org. Lett. 9 (2007) 1411.
[16] A. Pezzella, L. Panzella, A. Natangelo, M. Arzillo, A. Napolitano, M. d'Ischia, J. Org. Chem. 72 (2007) 9225.
[17] Y.V. Il'ichev, J.D. Simon, J. Phys. Chem. B 107 (2003) 7162.
[18] B.J. Powell, T. Baruah, N. Bernstein, K. Brake, R.H. McKenzie, P. Meredith, M.R. Pederson, J. Chem. Phys. 120 (2004) 8608.
[19] B.J. Powell, Chem. Phys. Lett. 402 (2005) 111.
[20] H. Okuda, A. Nakamura, K. Wakamatsu, S. Ito, T. Sota, Chem. Phys. Lett. 433 (2007) 355.
[21] M.L. Tran, B.J. Powell, P. Meredith, Biophys. J. 90 (2006) 743.
[22] E. Kaxiras, A. Tsolakidis, G. Zonios, S. Meng, Phys. Rev. Lett. 97 (2006) 218102.
[23] A. Pezzella et al., J. Am. Chem. Soc. 128 (2006) 15490.
[24] S. Meng, E. Kaxiras, Biophys. J. 94 (2008) 2095.
[25] S. Meng, E. Kaxiras, Biophys. J. 95 (2008) 4396.
[26] M. d'Ischia, O. Crescenzi, A. Pezzella, M. Arzillo, L. Panzella, A. Napolitano, V. Barone, Photochem. Photobiol. 84 (2008) 600.
[27] H. Okuda, K. Wakamatsu, S. Ito, T. Sota, J. Phys. Chem. A 112 (2008) 11213.

THE JOURNAL OF IMMUNOLOGY

Spatiotemporal Regulation of Heat Shock Protein 90-Chaperoned Self-DNA and CpG-Oligodeoxynucleotide for Type I IFN Induction via Targeting to Static Early Endosome

Koichi Okuya, Yasuaki Tamura, Keita Saito, Goro Kutomi, Toshihiko Torigoe, Koichi Hirata and Noriyuki Sato

J Immunol 2010;184;7092-7099; Prepublished online 14 May 2010;
doi:10.4049/jimmunol.1000490
http://www.jimmunol.org/content/184/12/7092

The Journal of Immunology is published twice each month by
The American Association of Immunologists, Inc.,
9650 Rockville Pike, Bethesda, MD 20814-3994.

Print ISSN: 0022-1767 Online ISSN: 1550-6606.

Spatiotemporal Regulation of Heat Shock Protein 90-Chaperoned Self-DNA and CpG-Oligodeoxynucleotide for Type I IFN Induction via Targeting to Static Early Endosome

Koichi Okuya,*,† Yasuaki Tamura,* Keita Saito,*,† Goro Kutomi,† Toshihiko Torigoe,* Koichi Hirata,† and Noriyuki Sato*

Recent studies have suggested that TLR9 signaling in early endosomes leads to IFN-α production by plasmacytoid dendritic cells (pDCs), whereas TLR9 signaling in late endosomes induces pDC maturation, IL-6, and TNF-α secretion. In this study, we show that human DNA as well as CpG-oligodeoxynucleotides (ODNs) in complex with heat shock protein 90 (Hsp90) stimulate pDCs to produce large quantities of IFN-α. The Hsp90–CpG-A complexes are targeted into the Rab5$^+$, early endosomal Ag 1$^+$-static early endosome postinternalization by DCs, suggesting that preferential sorting of Hsp90-chaperoned self-DNA/CpG-ODNs to the static endosome is required for signaling through TLR9 for IFN-α production. Interestingly, Hsp90-mediated preferential static early endosomal translocation of CpG-ODNs triggers robust IFN-α production from murine conventional DCs. Thus, extracellular Hsp90 converts inert self-DNA/CpG-ODNs into a potent trigger of IFN-α production via spatiotemporal regulation. ***The Journal of Immunology*****, 2010, 184: 7092–7099.**

Heat shock proteins (HSPs) are molecular chaperones that control the folding and prevent the aggregation of proteins. It is well known that tumor-derived HSPs, such as Hsp70, Hsp90, and gp96, initiate efficient tumor-specific CTL responses and protective immunity (1–6). We have demonstrated that extracellular HSP–Ag peptide complexes are efficiently cross-presented via the endosome–recycling pathway (7, 8). In this HSP-mediated cross-presentation, the receptor-dependent endocytosed HSP–peptide complex is translocated to the early endosome, and thereafter, the Hsp90-chaperoned peptide is transferred onto recycling MHC class I molecules.

Bacterial and viral DNAs rich in CpG motifs or small synthetic oligodeoxynucleotides (ODNs) containing CpG motifs activate innate immune cells, such as dendritic cells (DCs), via TLR9 (9, 10). TLR9 is expressed within endolysosomal compartments in innate immune cells and recognizes distinct patterns of nucleic acids in the endolysosomal compartments (11–15). Upon TLR9 engagement, IFN-α induction depends on the MyD88–IFN regulatory factor (IRF)-7 signaling pathway (16, 17). DC subpopulations are characterized by expression of different surface markers and the ability to produce cytokines that modulates both innate resistance and the adaptive immune response (18). In the murine system, the plasmacytoid DCs (pDCs) are CD11c^{low} B220^{high} Ly6C^{high} cells exhibiting plasmacytoid morphology and are able to produce a high level of IFN-α in response to several viruses or to CpG-ODN (19–21). Murine CD11c^{high} conventional DCs (cDCs) have been further subdivided into subsets, such as CD8$^+$ DCs and CD8$^-$ DCs (18). In humans, CD11c$^-$ IL-3R^{high} pDCs differ from CD11c$^+$ myeloid DCs (mDCs) in being uniquely able to produce a large amount of IFN-α in response to viral stimulation (22, 23) or to CpG-ODN (24). Previous studies revealed that CpG-A or various DNAs needed to be retained for long periods in the endosomes of pDCs for sufficient activation of TLR9 signaling (25, 26). Recently, CpG-ODNs have shown promising results as vaccine adjuvants for cancer immunotherapy due to their ability to induce potent Th1-type immune responses and anti-tumor responses (27–30).

Very recently, Lakadamyali et al. (31) have shown that early endosomes are comprised of two distinct populations called static early endosomes, which are slow maturing, and rapidly maturing dynamic early endosomes.

We have demonstrated that targeting of HSP–peptide complexes to the early endosomal Ag 1 (EEA1)$^+$, Rab5$^+$-static early endosome is crucial for cross-presentation (8).

In this study, we show that Hsp90 can form complexes with CpG-ODNs in vitro and that these complexes act as potent inducers of IFN-α production not only by pDCs but also cDCs. Furthermore, we show that extracellular CpG-ODN–Hsp90 complexes accumulate in the static early endosome but not the dynamic early endosome when pulsed onto DCs. In the human system, Hsp90 can convert inert self-DNA into a potent trigger of IFN-α production by targeting static early endosomes via spatiotemporal regulation. Thus, extracellular Hsp90 can be an excellent immunomodulator for cancer immunotherapy via spatiotemporal regulation of chaperoned molecules.

Materials and Methods

Mice

C57BL/6 mice were obtained from The Jackson Laboratory (Bar Harbor, ME). *Tlr9*$^{-/-}$ mice were kindly provided by Dr. S. Akira (Osaka University, Osaka, Japan). All mice were kept in a specific-pathogen-free

*Department of Pathology and †Department of Surgery, Sapporo Medical University School of Medicine, Sapporo, Japan

Received for publication February 12, 2010. Accepted for publication April 14, 2010.

This work was supported in part by Grant-in-Aid for Scientific Research and Program for developing the supporting system for upgrading the education and research from the Ministry of Education, Culture, Sports, Science and Technology and Health and Labor Sciences Research Grant-in Aid from the Ministry of Health, Labor, and Welfare of Japan.

Address correspondence and reprint requests to Dr. Yasuaki Tamura, Sapporo Medical University School of Medicine, S1W17, Chuo-ku, Sapporo, Hokkaido 060-8556, Japan. E-mail address: ytamura@sapmed.ac.jp

The online version of this article contains supplemental material.

Abbreviations used in this paper: cDC, conventional dendritic cell; DC, dendritic cell; EEA1, early endosomal Ag 1; ER, endoplasmic reticulum; HSP, heat shock protein; IRF, IFN regulatory factor; LAMP1, lysosome-associated membrane protein 1; mDC, myeloid DC; ND, not detected; NS, normal saline; ODN, oligodeoxynucleotide; pDC, plasmacytoid dendritic cell; SLE, systemic lupus erythematosus.

www.jimmunol.org/cgi/doi/10.4049/jimmunol.1000490

mouse facility. Studies were performed by an approval of Animal Experiment Ethics Committee of Sapporo Medical University (Sapporo, Japan).

Oligodeoxynucleotides

Synthesized CpG ODNs were purchased from Sigma-Aldrich (St. Louis, MO) and Invivogen (San Diego, CA). The sequences of ODNs were: murine CpG-A, 5′-ggTGCATCGATGCAgggggG-3′; murine CpG-B, 5′-tccatgacgttcctgatgct-3′; and control CpG ODN, 5′-ggTGCATGCATGCA-gggggg-3′. ODN2216 was CpG ODN type A-human TLR9 ligand (5′-ggGGGACGATCGTCgggggg-3′) and purchased from Invivogen.

Protein and Abs

Purified human Hsp90 was purchased from Stressgen (Ann Arbor, MI). Organelles were detected by laser confocal microscopy with specific Abs against KDEL (Stressgen) for endoplasmic reticulum (ER), Rab5 (Santa Cruz Biotechnology, Santa Cruz, CA) and EEA1 (Abcam, Cambridge, MA) for early endosomes, and lysosome-associated membrane protein 1 (LAMP1) (Santa Cruz Biotechnology) for lysosomes. Each Ab was labeled with Alexa Fluor 488 or Alexa Fluor 594 (Molecular Probes, Eugene, OR). Alexa Fluor 488 was used for labeling Hsp90.

Preparation of DCs

Murine cDCs and pDCs were isolated from bone marrow-derived DCs using magnetic beads and the MACS system (Miltenyi Biotec, Auburn, CA). Bone marrow cells were cultured for 5 d in a 5% CO_2 environment at 37°C in complete RPMI 1640 medium with 10% FCS, 20 ng/ml GM-CSF (Endogen, Woburn, MA), and 50 μM 2-ME (Invitrogen, Carlsbad, CA). Murine pDCs were purified using a Plasmacytoid Dendritic Cell Isolation Kit (Miltenyi Biotec), and cDCs were purified by negative selection with anti-murine pDC Ag 1 microbeads (Miltenyi Biotec), followed by positive selection with CD11c beads (Miltenyi Biotec). To confirm the expression of TLR9 and IRF7, pDCs and cDCs were lysed with 0.5% CHAPS containing protease inhibitor (Roche, Basel, Switzerland). Equal amounts of protein were separated by SDS-PAGE and analyzed by immunoblotting with anti-TLR9 (Invivogen), anti-IRF7 (Abcam), and β-actin Abs (Sigma-Aldrich). For RT-PCR, RNA was isolated from pDCs and mouse spleen cells using an RNeasy mini kit (Qiagen, Valencia, CA). Cells were pelleted at 4°C and resuspended in RLT lysis buffer (Qiagen). Total RNA was extracted following on-column DNase digestion using RNeasy mini columns and collected in RNase-free water. Oligo(dT)-primed reverse transcriptase of RNA into cDNA was performed with a Superscript III first-strand synthesis kit (Invitrogen), and 5% of the product was used for each RT-PCR sample using PCR buffer with hot-start Invitrogen Taq polymerase (Invitrogen). Primer pairs for TLR9 (forward 5′-GCTTT-GGCCTTTCACTCTTG-3′ and reverse 5′-AACTGCGCTCTGTGCC-TTAT-3′) and GAPDH (forward 5′-GAGTCAACGGATTTGGTCGT-3′ and reverse 5′-TTGATTTTGGAGGGATCTCG-3′) were designed using Primer3. Human mDCs and pDCs were isolated from PBMCs of healthy donors with mDC and pDC isolation kits (Miltenyi Biotec) according to the manufacturer's instructions.

Generation of CpG-ODN–Hsp90 complex in vitro

To confirm whether CpG-ODN–Hsp90 complexes could be generated, 1.5 nmol CpG-ODN was end labeled with T4-polynucleotide kinase and γ[^{32}P]-ATP, followed by incubation with 0.5 μM purified Hsp90 (Stressgen) at 37°C for 30 min. These samples were then separated by native-PAGE, and the gels were analyzed with silver staining and exposed to a Fuji BAS-MS imaging plate (Fuji Medical Systems, Tokyo, Japan) for ~24 h. The images were scanned using a BAS-2500 Phosphor Imaging System (Fuji Medical Systems). To make 3 μM CpG-ODN–Hsp90 complex, 3 nmol CpG-ODN was mixed with 1 μM Hsp90, incubated for 30 min, and then diluted with 1 ml medium.

Measurement of cytokine production

DCs were plated at 5–10 × 10^4 cells/well in flat-bottomed, 96-well plates in 100 μl complete RPMI 1640 medium with 10% FCS and stimulated with various reagents for 24 h. CpG–ODN or CpG-ODN–Hsp90 complex was added to medium at a final concentration of 3 μM. Supernatants were diluted and tested for various cytokines with mouse or human IFN-α (PBL InterferonSource, Piscataway, NJ), TNF-α (Pierce, Rockford, IL), and IL-6 (R&D Systems, Minneapolis, MN) using a sandwich ELISA kit. Absorbance was determined at 450 nm.

Flow cytometry

For detection of cell surface-bound and intracellular CpG-A that was transported by cDC and pDC, isolated mouse cDCs and pDCs were incubated with synthesized Cy5-labeled CpG-A (Sigma-Aldrich) or a complex with Hsp90 at 37°C. After 30 min, flow cytometric analysis was performed on an FACSCaliber flow cytometer (BD Biosciences, San Jose, CA).

Confocal imaging

Hsp90 was conjugated with Alexa Fluor 488 (Molecular Probes) according to the manufacturer's instructions. To visualize the kinetics of exogenously loaded Hsp90, purified cDCs were seeded on glass coverslips for 12 h and were first incubated with Alexa Fluor 488-labeled Hsp90 (10 μg) at 4°C for 10 min and washed. The cells were then further incubated for 0–120 min, fixed with 4% paraformaldehyde for 5 min at room temperature, and visualized. For the detection of colocalization with exogenous Hsp90 and organelles, cDCs were incubated with Alexa Fluor 488-labeled Hsp90 at 37°C for 120 min and washed. The cells were then fixed with 4% paraformaldehyde, permeabilized with 0.1% Triton X-100, and then blocked with 10% goat serum for 40 min. Cells were stained with anti-KDEL for detecting ER, anti-LAMP1 for late endosomes and lysosomes, and anti-Rab5 and anti-EEA1 for early endosomes for 60 min, followed by Alexa Fluor 594-conjugated goat anti-rabbit IgG for 60 min, and mounted. To analyze the intracellular routing of CpG-A, cDCs were seeded on glass coverslips for 12 h and stimulated with Cy5-labeled CpG-A alone for 30 min. Then the cells were washed and incubated with medium without CpG-A for 0, 60, and 120 min, fixed, permeabilized with 0.1% Triton X-100, and blocked with 10% goat serum for 40 min. Following this, they were stained with anti-EEA1 and anti-LAMP1 Abs followed by Alexa Fluor 488-conjugated goat anti-rabbit IgG. To analyze the intracellular routing of complexed CpG-A with Hsp90, cDCs were seeded on glass coverslips for 12 h and stimulated with complexed Cy5-labeled CpG-A with Hsp90 for 30 min. Then the cells were washed and incubated with medium without CpG-A for 0, 60 and 120 min, fixed with 4% paraformaldehyde, permeabilized with 0.1% Triton X-100 and blocked with 10% goat serum for 40 min. Following this, they were stained with anti-Rab5, anti-EEA1, and anti-LAMP1 Abs followed by Alexa Fluor 488-conjugated goat anti-rabbit IgG. All samples were visualized using an LSM510 confocal microscope (Zeiss, Oberkochen, Germany), and images were captured and analyzed using the Zeiss LSM Image Browser (Zeiss). For evaluation of colocalization, a single z-plane of one cell was evaluated. For each protein and organelle combination, a total of 150 cells (50 cells each from three independent experiments) were analyzed.

Mouse injections

For analysis of in vivo cytokine production induced by stimulation with CpG-A, C57BL/6 mice were anesthetized and challenged with normal saline (50 μl), Hsp90 (20 μg/mouse), CpG-A (50 μg/mouse), and CpG-A (50 μg) complexed with Hsp90 (20 μg) by the i.p. route. After 12 h, blood was collected by cardiac puncture, and serum was prepared for IFN-α ELISA. Spleens were collected and crushed for isolation of spleen cells, and cDCs were enriched by negative selection using anti-murine pDC Ag 1 microbeads, followed by positive selection using anti-CD11c microbeads, and cultured for 24 h. Supernatants were then collected for IFN-α ELISA.

Genomic DNA isolation

Human genomic DNA was isolated from PBMCs of healthy donors using a DNeasy kit (Qiagen) according to the manufacturer's instructions.

Statistical analysis

All experiments were independently performed three times in triplicate. Results were given as means + SEM. Comparisons between two groups were performed using Student t test, whereas comparisons among multiple groups were done using ANOVA, with a value of $p < 0.05$ considered to be statistically significant.

Results

Extracellulary loaded Hsp90 accumulates in static early endosomes within cDCs

We first examined the intracellular trafficking of extracellular Hsp90 loaded onto cDCs. We labeled native Hsp90 protein with Alexa Fluor 488 and loaded it onto cDCs separated from mouse bone marrow-derived DCs using an anti-CD11c Ab at 4°C for 10 min and washed. The cells were then further incubated for 0–120 min, and we analyzed the kinetics of intracellular trafficking of Hsp90. Extracellular Hsp90 was gradually trafficked from the cell surface to the cytosol with the passage of time (Fig. 1*A*). To

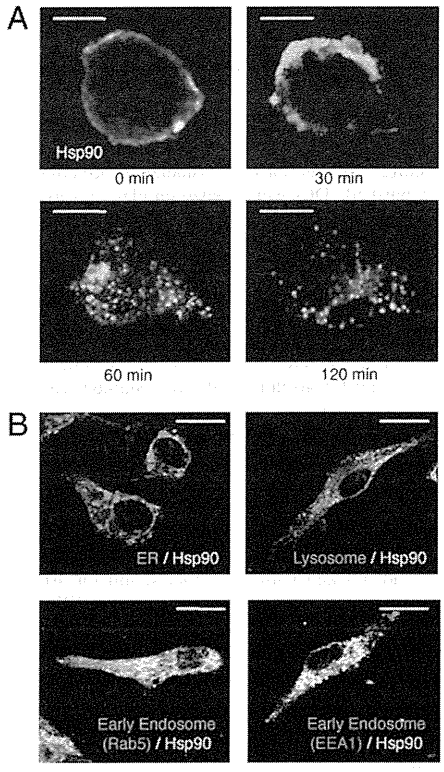

FIGURE 1. Extracellulary loaded Hsp90 accumulates in the static early endosome. *A*, Isolated murine cDCs were loaded with Alexa Fluor 488-labeled Hsp90 (10 μg) at 4°C for 10 min and washed. The cells were then further incubated for 0–120 min and fixed with 4% paraformaldehyde, and then visualized by laser confocal microscopy (original magnification ×630). Bar, 5 μm. *B*, Isolated cDCs were pulsed with Alexa Fluor 488-labeled Hsp90 for 2 h. Postincubation, the cells were fixed and stained with anti-KDEL (for ER), anti-LAMP1 (for late endosomes and lysosomes), anti-Rab5 (for early endosomes), and anti-EEA1 (for static early endosomes) followed by Alexa Fluor 594-conjugated goat anti-rabbit IgG or anti-mouse IgG, and then visualized by laser confocal microscopy (original magnification ×630). Bar, 10 μm. Data in *A* and *B* are representative of three independent experiments.

investigate the intracellular localization of extracellular Hsp90, cDCs were incubated with the Alexa Fluor 488-labeled Hsp90 for 30 min and washed. Postincubation with medium without Hsp90 for 120 min, the cells were fixed and stained with organelle markers, such as KDEL for ER, LAMP1 for the late endosome and lysosome, and Rab5 and EEA1 for the early endosome. Extracellular Hsp90 accumulated in Rab5 and EEA1 positive-early endosomes but not in ER or late endosomes/lysosomes (Fig. 1*B*). These results indicated that extracellular Hsp90 was sorted into the static early endosomal pathway and retained for longer periods, but not the dynamic early endosomal pathway. These observations led us to investigate whether extracellular Hsp90 converted non–IFN-α stimulatory CpG-A ODN into a trigger of cDC activation to produce IFN-α.

In vitro generation of CpG-ODN–Hsp90 complex

As Hsp90 has been demonstrated to be a binder to CpG-ODNs (32), we first confirmed whether Hsp90 could be complexed with CpG-A and control CpG in vitro. We incubated 1.5 nmol end labeled CpG-ODN with 0.5 μM Hsp90 at 37°C for 30 min. Samples were subjected to native-PAGE and visualized by silver staining (Fig. 2*A*) and autoradiograpy (Fig. 2*B*). These results indicated that Hsp90 could bind CpG-ODNs. To make a 3 μM CpG-ODN–Hsp90 complex, 3 nmol CpG-A or CpG-B was mixed with 1 μM Hsp90, incubated for 30 min, and then diluted with 1 ml medium.

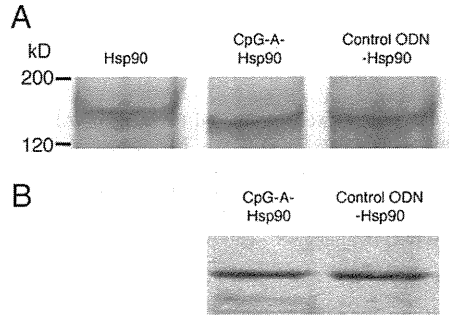

FIGURE 2. In vitro generation of CpG-ODN–Hsp90 complex. Purified Hsp90 (0.5 μM) and CpG-DNA (1.5 nmol) that were end labeled with T4-polynucleotide kinase and ($\gamma[^{32}P]$)-ATP were incubated at 37°C for 30 min. Samples were separated by native-PAGE. *A*, The gels were analyzed using silver staining. *B*, The gels were exposed to a Fuji BAS-MS imaging plate (Fuji Medical Systems) for 24 h, and the images were scanned using the Phosphor Imaging System (Fuji Medical Systems).

Hsp90 enhances IFN-α induction in response to CpG-A from pDC and cDC

Mouse pDCs, not cDCs, have previously been demonstrated to be the major cells secreting IFN-α following CpG-A stimulation. To elucidate the ability of Hsp90 to enhance secretion of IFN-α from the DC subset, freshly isolated pDCs were cultured for 24 h in the presence of 3 μM CpG-A or 3 μM CpG-A–Hsp90 complex, respectively. The CpG-A–Hsp90 complex enhanced the IFN-α production 2-fold more than CpG-A alone (Fig. 3*A*). Notably, a high amount of IFN-α production was observed in cDCs stimulated with the CpG-A–Hsp90 complex despite the lack of production of IFN-α

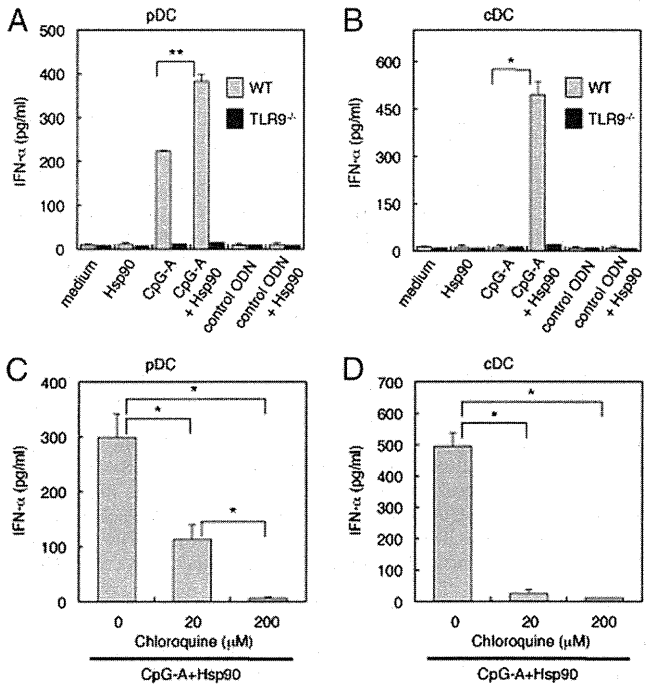

FIGURE 3. CpG-A–Hsp90 complexes enhance induction of IFN-α by DCs in vitro. IFN-α production poststimulation with 3 μM CpG-A, control ODN alone, or in complex with Hsp90 by pDCs from WT and *Tlr9*$^{-/-}$ mice (*A*) and cDCs from WT and *Tlr9*$^{-/-}$ mice (*B*). The effect of chloroquine treatment on IFN-α production poststimulation with 3 μM CpG-A–Hsp90 complex by pDCs (*C*) and cDCs (*D*). IFN-α production was determined by ELISA. Data are presented as means + SEM of triplicate wells. Data are representative of three independent experiments. $*p < 0.0005$; $**p < 0.001$, paired Student *t* test.

when they were stimulated with CpG-A alone (Fig. 3*B*). Exogenous Hsp90 did not have any effect on IFN-α secretion by either pDCs or cDCs (Fig. 3*A*, 3*B*). Furthermore, the observed IFN-α production was completely inhibited poststimulation with the CpG-A–Hsp90 complex in both pDCs and cDCs derived from *Tlr9*$^{-/-}$ mice (Fig. 3*A*, 3*B*). Moreover, IFN-α production was potently inhibited by chloroquine, which blocks endosomal signaling (Fig. 3*C*, 3*D*). The degree of the inhibition of the IFN-α production by chloroquine was different between pDCs and cDCs, but this may have been due to the sensitivity to the chloroquine. These results suggested that Hsp90 might translocate the chaperoned CpG-ODNs into static early endosomes and efficiently activate the TLR9 signaling pathway for IFN-α production.

Both cDCs and pDCs uptake CpG-A to similar degrees

We compared the efficiency of binding and uptake of CpG-A or the CpG-A–Hsp90 complex by cDCs and pDCs to rule out the possibility that Hsp90 enhanced the uptake of CpG-A by cDCs and pDCs. Cy5-labeled CpG-A, either coupled with Hsp90 or alone, was added to cDC or pDC cultures, and the binding and uptake were analyzed. The percentage of cDCs that took-up CpG-A was 36.9% with CpG-A stimulation alone, and it was approximately the same, 39.5%, when it was coupled with Hsp90 (Fig. 4). The uptakes of CpG-A alone and the CpG-A–Hsp90 complex by pDCs were also similar. These results indicated that both cDCs and pDCs took up the labeled CpG-ODN at almost the same level and supported our hypothesis that Hsp90-mediated direction of CpG-A into the early endosome might be essential for IFN-α production in cDCs.

Mouse cDCs express TLR9 and IRF7

We examined whether TLR9 was expressed by murine cDCs. TLR9 protein and mRNA expression were determined by immunoblot and RT-PCR analyses using freshly isolated highly purified cDCs populations (Supplemental Fig. 1*A*, 1*B*). Laser confocal microscopic analysis revealed that TLR9 localized in the EEA1-positive early endosomes of cDCs (Supplemental Fig. 1*C*).

CpG-ODN–Hsp90 complex serves as a potent inducer for IFN-α in vivo

Next, we examined whether the CpG-A–Hsp90 complex had an in vivo effect similar to that observed in vitro. We administered PBS, Hsp90 alone, CpG-A alone, or the CpG-A–Hsp90 complex to C57BL/6 mice. After 12 h, we collected sera from the mice and measured the IFN-α. The production of IFN-α from mice injected with the CpG-A–Hsp90 complex was higher than that induced by CpG-A alone (Fig. 5*A*). Moreover, production of IFN-α by cDCs isolated from spleens of treated mice and cultured ex vivo for 40 h was measured. cDCs isolated from mice injected with the CpG-A–Hsp90 complex produced a high level of IFN-α. In contrast, cDCs from mice injected with CpG-A alone did not (Fig. 5*B*). These results indicated that Hsp90 could target chaperoned molecules to the early endosomal compartment within cDCs and induce robust INF-α secretion in vivo as well as in vitro.

Hsp90 retains CpG-ODN in static early endosomes

We assumed that in cDCs, as CpG-A was rapidly trafficked to late endosomes and lysosomes, CpG-A–mediated TLR9 signaling was not sufficient. We therefore investigated the intracellular routing of CpG-A after uptake of it in cDCs using laser confocal microscopy. Isolated cDCs from BMDCs were incubated with Cy5-labeld CpG-A for 30 min, and then the cells were washed and incubated with new medium without CpG-A for 0, 60, and 120 min. Following incubation, the cells were fixed and stained. Immediately poststimulation, most of the CpG-A localized within LAMP1$^+$ late endosomes/lysosomes (Fig. 6*A*, Supplemental Fig. 2). In contrast, the frequency of colocalization with EEA1 was very low. After 120 min incubation, CpG-A was detected within late endosmes/lysosomes at high frequency and in a large area of the LAMP1$^+$ organelle (Fig. 6*A*, Supplemental Fig. 2). Together with our observation that TLR9 localized in the EEA1 positive-early endosomes of cDCs, these results indicated that CpG-A was rapidly trafficked to the LAMP1$^+$ late endosme/lysosome pathway, and therefore could not activate the TLR9–MyD88–IRF7 signaling pathway. In contrast, Cy5-labeled CpG-A coupled with Hsp90 was pooled for at least 120 min during stimulation within Rab5$^+$, EEA1$^+$-static early endosomes, and lysosomal localization was poorly detected (Fig. 6*B*, Supplemental Fig. 3). Furthermore, when complexed with Hsp90, CpG-A appeared to form large aggregates that colocalized with early endosomes after 120 min (Fig. 6*B*). These results suggested that their ability to form aggregated structures was needed to induce IFN-α. Quantitative analysis of the colocalization between the Cy5-labeled CpG-A and EEA1 and LAMP1 revealed average colocalization incidences of 16.7% and 91.9%, respectively, immediately after

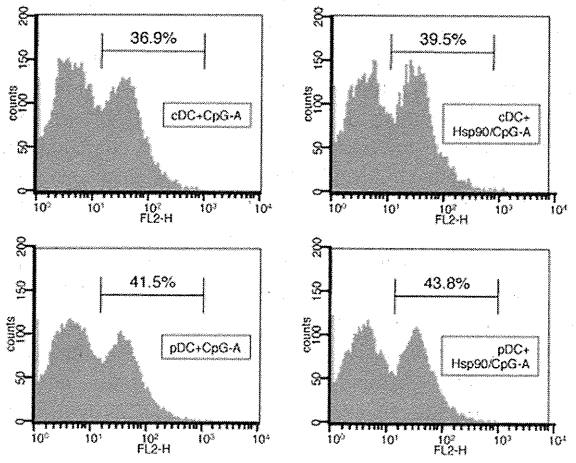

FIGURE 4. Both pDCs and cDCs bind and uptake CpG-A or Hsp90–CpG-A complex to similar degrees. Flow cytometric analysis for binding and uptake of Cy5-labeled CpG-A alone (*left panels*) or in complex with Hsp90 (*right panels*) by cDCs (*top panels*) and pDCs (*bottom panels*) after 30 min stimulation. Data are representative of three independent experiments.

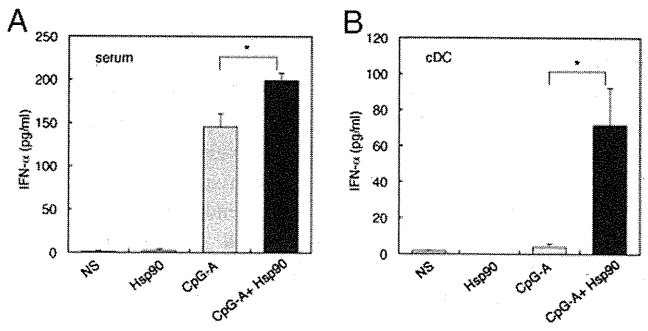

FIGURE 5. CpG-A–Hsp90 complex serves as a potent inducer for IFN-α in vivo. CpG-A (50 μg/mouse) or CpG-A–Hsp90 (50 μg/mouse) complex was administered i.p. to C57BL/6 mice 6–10 wk of age. *A*, After 12 h, mouse serum was obtained via cardiac puncture and levels of IFN-α were measured using ELISA. *B*, Mice were then euthanized for spleen removal. cDCs were isolated and cultured for 24 h, and the supernatant was measured for IFN-α production. Data are presented as means + SEM of triplicate wells. Data are representative of three independent experiments. *$p < 0.01$; paired Student t test.

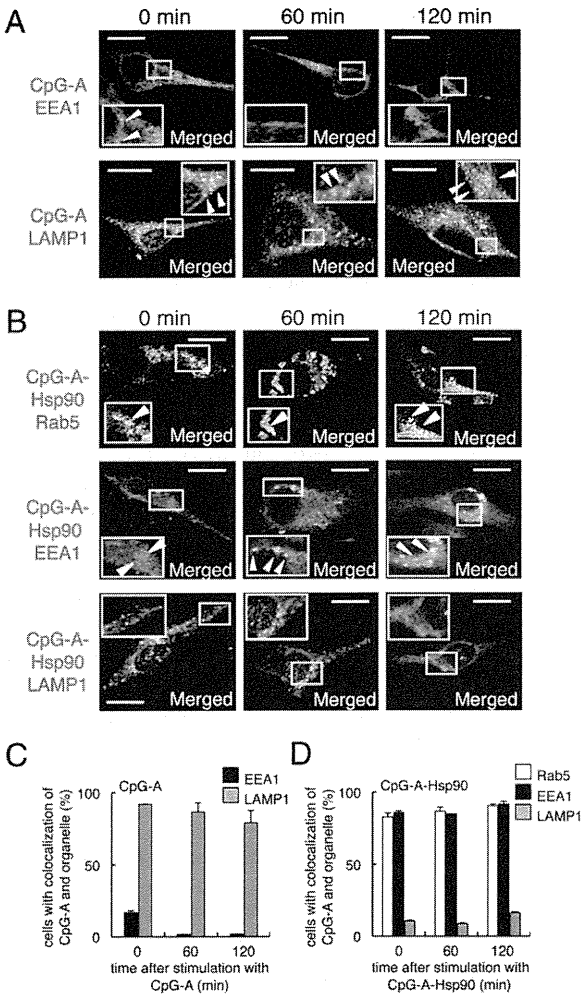

FIGURE 6. Hsp90 targets CpG-A to the early endosome for longer periods. Isolated cDCs were pulsed with 3 μM Cy5-labeled CpG-A (*A*) or 3 μM Cy5-labeled CpG-A–Hsp90 complex (*B*) for 30 min. Postincubation with new medium without CpG-A for 0, 60, and 120 min, the cells were fixed, stained, and then visualized by laser confocal microscopy (original magnification ×630). Arrowheads indicate colocalization of CpG-A and each organelle. Bar, 10 μm. Data are representative of three independent experiments. For evaluation of colocalization, a single *z*-plane of one cell was evaluated. For each CpG-A (*C*) or CpG-A–Hsp90 complex (*D*) and organelle combination, a total of 150 cells (50 cells each from three independent experiments) were analyzed.

CpG-A stimulation, which changed to 1.7% and 78.9%, respectively, with the passage of time (Fig. 6*C*). In contrast, the colocalization rates between the Cy5-labeled CpG-A that formed a complex with Hsp90 and Rab5, EEA1, and LAMP1 were 90.6%, 91.5%, and 16.2%, respectively, at 2 h after CpG-A sitimulation (Fig. 6*D*). These data suggested that Hsp90 could target CpG-A to the static early endosome, resulting in efficient TLR9 stimulation for a high amount of IFN-α production by cDCs. Thus, Hsp90 had the ability to retain CpG-ODNs for longer periods in the static early endosome, presumably enabling the selective and continuous activation of early endosomal TLR9 via spatiotemporal targeting of CpG-ODNs.

Extracellular Hsp90 converts CpG-B into a trigger of IFN-α production by cDCs

Recent studies have indicated that TLR9 signaling in late endosomes induces DC maturation and TNF-α and IL-6 secretion. We therefore tested whether Hsp90 could convert CpG-B, which was expected to stimulate TLR9 in late endosomes, into a ligand that triggered TLR9 in early endosomes to produce IFN-α. When complexed with Hsp90, CpG-B induced robust IFN-α production from cDCs (Fig. 7*A*) and only low levels of TNF-α and IL-6 as compared with CpG-B alone (Fig. 7*B*, 7*C*). The CpG-B–Hsp90 complex also failed to induce cDC maturation (data not shown). Consistent with these results, the production of TNF-α and IL-6 from cDCs was inhibited when they were stimulated with the CpG-A–Hsp90 complex as compared with CpG-A alone (Supplemental Fig. 4).

Extracellular Hsp90 enhances the IFN-α production by human pDCs

In humans, pDCs and B cells express TLR9 (10, 33). We examined whether the CpG-A–Hsp90 complex also induced IFN-α from human DCs as observed in mouse DCs. The production of IFN-α when we stimulated PBMCs of healthy donors with the CpG-A–Hsp90 complex was enhanced when compared with CpG-A alone ($p < 0.05$) (Fig. 8*A*). We observed that PBMC-derived mDCs expressed little TLR9 and that $CD19^+$ B cells expressed TLR9 at a low level (data not shown). Therefore, it was reasonable that there was little IFN-α production by these cells following stimulation with CpG-A or the CpG-A–Hsp90 complex (Fig. 8*B*, 8*C*). In contrast, as pDCs isolated from PBMCs have been shown to produce large amounts of IFN-α, we examined whether Hsp90 could affect the IFN-α production by human pDCs. The CpG-A–Hsp90 complex induced augmented production of IFN-α compared with CpG-A alone (Fig. 8*D*). We therefore concluded that Hsp90-mediated spatiotemporal targeting to static early endosomes of CpG-ODN boosted TLR9 activation and triggered efficient IFN-α induction in mouse pDCs, cDCs, and human pDCs.

Hsp90 converts self-DNA into a potent trigger of IFN-α induction by human pDCs

Finally, we determined whether the extracellular Hsp90 enabled human pDCs to sense self-DNA, leading to IFN-α production. Human genomic DNA, which was isolated from healthy volunteers, was unable to induce IFN-α from pDCs. However, we found that self-DNA complexed with Hsp90 could induce IFN-α production from pDCs (Fig. 9). Thus, Hsp90 converted inert self-DNA into an activator of pDCs.

Discussion

pDCs sense certain viral and microbial infections. In contrast to mDCs, pDCs uniquely express TLR7 and TLR9, intracellular receptors that recognize viral/microbial nucleic acids within endosomal compartments in humans. Together with the constitutive expression of IRF7, TLR7 and TLR9 permit pDCs to mount rapid and robust type I IFN responses to viral/microbial infections. However, pDCs normally do not respond to self-DNA, which may reflect the fact that viral/bacterial DNA sequences contain multiple CpG nucleotides that bind and activate TLR9, whereas mammalian self-DNA contains fewer such motifs, which are most likely masked by methylation. Recent evidence, however, suggests that self-DNA has the potential to trigger TLR9, but may fail to do so because it fails to access the TLR9-containing endolysosomal compartments. One of the mechanisms of this effect is attributed to the fact that DNase easily and rapidly breaks down the extracellular DNA, thereby hampering self-DNA localization into endocytic compartments. In contrast to the human system, murine cDCs, like pDCs, express TLR7 and TLR9.

Two classes of synthetic ODNs containing an unmethylated CpG motif have been classified: CpG-A ODN, which stimulates IFN-α production by pDCs, and CpG-B ODN, which does not. Instead, CpG-B ODN stimulates pDCs to produce IL-6 and TNF-α and induce DC maturation, such as the upregulation of CD80 and

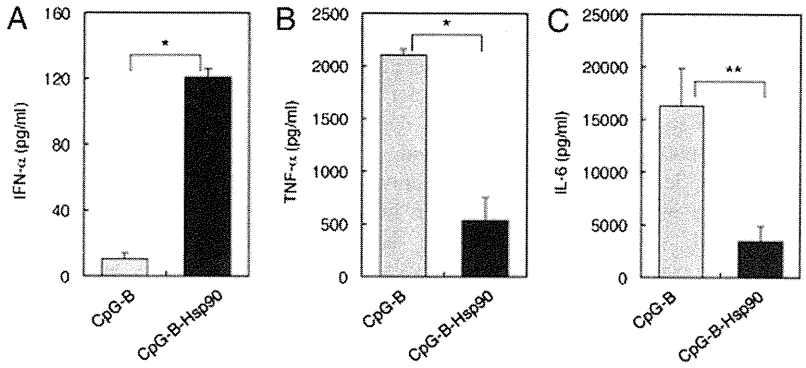

FIGURE 7. Hsp90 converts CpG-B to a trigger of IFN-α production by cDCs. IFN-α (*A*), TNF-α (*B*), and IL-6 (*C*) production poststimulation with 3 μM CpG-B or in complex with Hsp90 by cDCs. Data are presented as means + SEM of triplicate wells. Data are representative of three independent experiments. $*p < 0.005$; $**p < 0.01$, paired Student *t* test.

CD86 and the expression of MHC class II molecules. Recently, it has been demonstrated that the manner of CpG internalization and the retention time of CpG in endosomes differ between CpG-A and CpG-B, and the retention of the CpG/TLR9 complex in endosomes is the primary determinant of TLR signaling (17, 34). CpG-A ODNs are characterized by a poly G tail that forms large multimeric aggregates with a diameter ~50 μm. In contrast, CpG-B ODNs are monomeric and do not form such higher order structures. In addition, multimeric CpG-A ODNs are retained for longer periods of time in the early endosomes, whereas CpG-B ODNs rapidly traffic through early endosomes into late endosomes or lysosomes of pDCs. The prolonged retention of multimeric CpG-A ODNs provides extended activation of the TLR9-MyD88-IRF7 signal-transducing complex, which leads to robust IFN-α production. Therefore, we also examined the ability of Hsp90 to target and retain chaperoned CpG-DNA in static early endosomes of cDCs, resulting in type I IFN production. We found that Hsp90-chaperoned CpG-A was localized and retained within static early endosomes for longer periods in cDCs, thereby eliciting TLR9 signaling for IFN-α production, but not inflammatory cytokines, such as IL-6 and TNF-α. In contrast, CpG-A alone moved into late endosomes and lysosomes within cDCs. Interestingly, not only CpG-A but also CpG-B could stimulate the TLR9 signaling within static early endosomes, resulting in the production of IFN-α. Thus, extracellular Hsp90 had the ability to direct associated molecules into static early endosomes. Moreover, as time passed, the CpG-A–Hsp90 complex formed large aggregates within early endosomes (Fig. 6*B*), again suggesting an important link between the physical size of TLR9 ligands and their stimulatory capacity. Thus, our data indicated that when DCs detected aggregated DNA structures in the early endosomes through TLR9, this was coupled with IRF7 activation and IFN-α production. By contrast, when DCs sensed the linear DNA structures in the late endosomes or lysosomes through TLR9, this was coupled with NF-κB activation, which led to IL-6 and TNF-α production and DC maturation.

Why, however, are DNA–Hsp90 complexes selectively retained in early endosomes but not in late endosomes or lysosomes in DCs? We found that endocytosed CpG-A–Hsp90 complexes were selectively transferred into $Rab5^+$, $EEA\text{-}1^+$-static early endosomes. Very recently, Lakadamyali et al. (31) have shown that early endosomes are comprised of two distinct populations: a dynamic population that is highly mobile on microtubules and matures rapidly toward the late endosome and a static population that matures much more slowly. Cargos destined for degradation, including low-density lipoprotein, epidermal growth factor, and influenza virus, are internalized and targeted to the $Rab5^+$, $EEA1^-$ dynamic population of early endosomes, thereafter trafficking to $Rab7^+$ late endosomes. In contrast, the recycling ligand

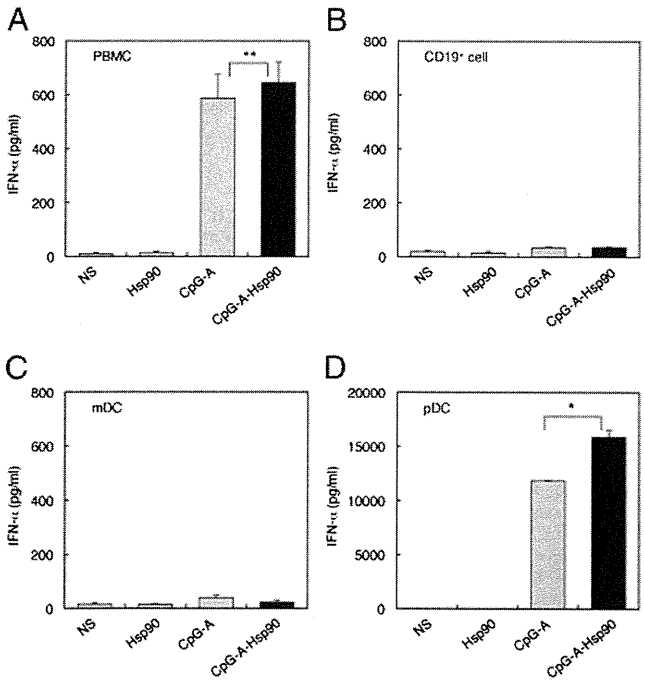

FIGURE 8. CpG-A–Hsp90 complex enhances IFN-α induction by human pDCs. IFN-α production poststimulation with NS, Hsp90, 3 μM CpG-A alone or in complex with Hsp90 by human PBMC (*A*), $CD19^+$ cells (*B*), mDCs (*C*), and pDCs (*D*). Data are presented as means + SEM of triplicate wells. Data are representative of three independent experiments. $*p < 0.005$, $**p < 0.05$, paired Student *t* test. NS, normal saline.

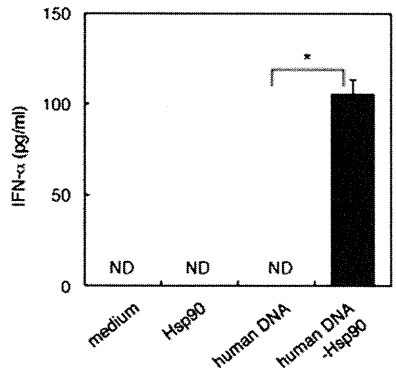

FIGURE 9. Hsp90 converts self-DNA into a potent trigger of IFN-α induction by human pDCs. Human pDCs were stimulated with genomic DNA isolated from healthy volunteers (10 μg/ml) either alone or postcomplexing with Hsp90 (10 μg). Levels of IFN-α were measured after overnight culture using ELISA. Error bars represent the SEM of triplicate wells. Data are representative of four independent experiments. $*p < 0.005$, paired Student *t* test. ND, not detected.

transferrin is delivered to $Rab5^+$, $EEA1^+$-static early endosomes, followed by translocation to $Rab11^+$ recycling endosomes. They also found that cargos trafficked into these static early endosomes were retained for longer periods and not translocated into late endosomes and lysosomes. Therefore, our observation that the CpG-A–Hsp90 complex was retained in the static early endosomes, leading to sustained activation of DCs and IFN-α production, was consistent with their findings. Moreover, as Rutz et al. (35) have demonstrated that TLR9–CpG ODN interaction occurs at the acidic pH (6.5–5.0) found in early endosomes and lysosomes but not at physiological pH (7.4), the Hsp90-mediated translocation of CpG-ODNs into static early endosomes (pH 6.5) might accelerate the TLR9 and CpG–ODN interaction. In contrast, CpG-A alone, which did not stimulate IFN-α production, targeted the $EEA1^-$ and $LAMP1^+$ dynamic early endosome-late endosome/lysosome pathway, leading to inflammatory cytokine responses as well as DC maturation through NF-κB–mediated signaling. These data suggested that Hsp90 shuttled the chaperoned DNA into the static early endosome, resulting in the formation of DNA aggregation under mildly acidic circumstances as well as preventing translocation to late endosomes/lysosomes. Therefore, we hypothesized that targeting of DNA to static early endosomes was critical for eliciting TLR9 signaling for IFN-α production by DCs. Furthermore, we examined whether Hsp90 could convert CpG-B, which is thought to stimulate TLR9 in late endosomes, into a ligand that triggers TLR9 in early endosomes. Indeed, when complexed with Hsp90, CpG-B induced pDCs to produce high levels of IFN-α of pDCs and only low levels of IL-6 and TNF-α as compared with CpG-B alone; the Hsp90 complexed with CpG-B also failed to induce pDC maturation as revealed by the low surface expression of CD80 and CD86. These data suggested that the CpG-B–Hsp90 complex made possible their retention in early endosomes and subsequent induction of higher levels of IFN-α and low levels of IL-6 and TNF-α and impaired pDC maturation.

Recently, it has been demonstrated that pDCs do sense and respond to self-DNA in human autoimmune diseases. In systemic lupus erythematosus (SLE), pDCs are activated to produce IFNs by circulating immune complexes consisting of autoantibodies and self-nucleic acids that stimulate endosomal TLR following FcγRII-mediated uptake. The aberrantly produced IFNs are major effectors in the pathogenesis of autoimmunity, mainly by inducing unabated maturation of peripheral mDCs that stimulate autoreactive T cells. Recent evidence implies that upon internalization of chromatin–IgG immune complexes via BCR or FcRIII of DCs, mammalian DNA displays robust immunostimulatory activities toward B cells or DCs (36, 37). Furthermore, the sera of patients with SLE containing immune complexes consisting of autologous DNA and anti-DNA Abs effectively activate pDCs to produce type I IFNs (38, 39). We have demonstrated that, upon Hsp90-mediated enforced endosomal translocation, both human self-DNA as well as CpG-ODN could activate DCs via TLR9 to produce type I IFN. Previous studies have demonstrated the presence of autoantibodies to the Hsp90 (40, 41) and enhanced expression of Hsp90 in PBMCs of patients with active SLE (42, 43), suggesting the role of Hsp90 in the pathogenesis. In addition, the Hsp90 has been shown to localize both in the cytoplasm and nucleus (44). Moreover, under stressful conditions, it has been shown that cytosolic Hsp90 translocates to the nucleus (45). This suggests that Hsp90 may bind self-DNA within the nucleus. When cells undergo necrosis, self-DNA associated with endogenous Hsp90 could be released into the extracellular space and might trigger IFN-α production by pDCs. Our findings support the idea that Hsp90, an endogenous danger signal found in the sera from patients with SLE, is the key mediator of pDC activation in SLE. Thus, Hsp90 may inactivate innate tolerance to self-DNA by forming a complex with self-DNA that is delivered to and retained within early endocytic compartments of pDCs to trigger TLR9 and induce IFN production. Thus, we determined a fundamental mechanism by which pDCs sense and respond to self-DNA coupled with Hsp90. Our data suggest that, through this pathway, pDCs drive autoimmunity in autoimmune diseases.

The release of host-derived (self) DNA into the extracellular environment is a common feature of both necrotic and apoptotic cell death (46). However, extracellular self-DNA usually does not lead to innate immune activation because it is rapidly degraded by DNase and fails to access endosomal compartments of DCs where TLR9 is located. The importance of this mechanism in preventing autoimmune responses is shown by the fact that mice deficient in DNase 1 develop an SLE-like syndrome. Several host factors that can convert self-DNA into a trigger of DC activation have been reported. Endogenous anti-microbial peptide LL37 (also known as CAMP), autoantibodies, and high mobility group box 1 protein have been demonstrated to do so. In this study, we found that extracellular self-DNA acquires the ability to trigger activation of TLR9 in human pDC by forming a complex with the host-derived endogenous Hsp90.

Together, our findings indicate that the ability of Hsp90 to convert self-DNA into a trigger of high levels of IFN-α production depends on its capacity to concentrate and retain DNA in static early endosomes, presumably enabling the selective and sustained activation of early endosomal TLR9.

Acknowledgments

We thank Dr. S. Akira for providing $Tlr9^{-/-}$ mice.

Disclosures

The authors have no financial conflicts of interest.

References

1. Udono, H., and P. K. Srivastava. 1994. Comparison of tumor-specific immunogenicities of stress-induced proteins gp96, hsp90, and hsp70. *J. Immunol.* 152: 5398–5403.
2. Tamura, Y., P. Peng, K. Liu, M. Daou, and P. K. Srivastava. 1997. Immunotherapy of tumors with autologous tumor-derived heat shock protein preparations. *Science* 278: 117–120.
3. Sato, K., Y. Torimoto, Y. Tamura, M. Shindo, H. Shinzaki, K. Hirai, and Y. Kohgo. 2001. Immunotherapy using heat-shock protein preparations of leukémia cells after syngeneic bone marrow transplantation in mice. *Blood* 98: 1852–1857.
4. Milani, V., E. Noessner, S. Ghose, M. Kuppner, B. Ahrens, A. Scharner, R. Gastpar, and R. D. Issels. 2002. Heat shock protein 70: role in antigen presentation and immune stimulation. *Int. J. Hyperthermia* 18: 563–575.
5. Noessner, E., R. Gastpar, V. Milani, A. Brandl, P. J. Hutzler, M. C. Kuppner, M. Roos, E. Kremmer, A. Asea, S. K. Calderwood, and R. D. Issels. 2002. Tumor-derived heat shock protein 70 peptide complexes are cross-presented by human dendritic cells. *J. Immunol.* 169: 5424–5432.
6. Ueda, G., Y. Tamura, I. Hirai, K. Kamiguchi, S. Ichimiya, T. Torigoe, H. Hiratsuka, H. Sunakawa, and N. Sato. 2004. Tumor-derived heat shock protein 70-pulsed dendritic cells elicit tumor-specific cytotoxic T lymphocytes (CTLs) and tumor immunity. *Cancer Sci.* 95: 248–253.
7. Kurotaki, T., Y. Tamura, G. Ueda, J. Oura, G. Kutomi, Y. Hirohashi, H. Sahara, T. Torigoe, H. Hiratsuka, H. Sunakawa, et al. 2007. Efficient cross-presentation by heat shock protein 90-peptide complex-loaded dendritic cells via an endosomal pathway. *J. Immunol.* 179: 1803–1813.
8. Kutomi, G., Y. Tamura, K. Okuya, T. Yamamoto, Y. Hirohashi, K. Kamiguchi, J. Oura, K. Saito, T. Torigoe, S. Ogawa, et al. 2009. Targeting to static endosome is required for efficient cross-presentation of endoplasmic reticulum-resident oxygen-regulated protein 150-peptide complexes. *J. Immunol.* 183: 5861–5869.
9. Wagner, H. 1999. Bacterial CpG DNA activates immune cells to signal infectious danger. *Adv. Immunol.* 73: 329–368.
10. Krieg, A. M. 2002. CpG motifs in bacterial DNA and their immune effects. *Annu. Rev. Immunol.* 20: 709–760.
11. Ahmad-Nejad, P., H. Häcker, M. Rutz, S. Bauer, R. M. Vabulas, and H. Wagner. 2002. Bacterial CpG-DNA and lipopolysaccharides activate Toll-like receptors at distinct cellular compartments. *Eur. J. Immunol.* 32: 1958–1968.

12. Heil, F., P. Ahmad-Nejad, H. Hemmi, H. Hochrein, F. Ampenberger, T. Gellert, H. Dietrich, G. Lipford, K. Takeda, S. Akira, et al. 2003. The Toll-like receptor 7 (TLR7)-specific stimulus loxoribine uncovers a strong relationship within the TLR7, 8 and 9 subfamily. *Eur. J. Immunol.* 33: 2987–2997.
13. Lee, J., T. H. Chuang, V. Redecke, L. She, P. M. Pitha, D. A. Carson, E. Raz, and H. B. Cottam. 2003. Molecular basis for the immunostimulatory activity of guanine nucleoside analogs: activation of Toll-like receptor 7. *Proc. Natl. Acad. Sci. USA* 100: 6646–6651.
14. Matsumoto, M., K. Funami, M. Tanabe, H. Oshiumi, M. Shingai, Y. Seto, A. Yamamoto, and T. Seya. 2003. Subcellular localization of Toll-like receptor 3 in human dendritic cells. *J. Immunol.* 171: 3154–3162.
15. Latz, E., A. Schoenemeyer, A. Visintin, K. A. Fitzgerald, B. G. Monks, C. F. Knetter, E. Lien, N. J. Nilsen, T. Espevik, and D. T. Golenbock. 2004. TLR9 signals after translocating from the ER to CpG DNA in the lysosome. *Nat. Immunol.* 5: 190–198.
16. Honda, K., H. Yanai, H. Negishi, M. Asagiri, M. Sato, T. Mizutani, N. Shimada, Y. Ohba, A. Takaoka, N. Yoshida, and T. Taniguchi. 2005. IRF-7 is the master regulator of type-I interferon-dependent immune responses. *Nature* 434: 772–777.
17. Honda, K., Y. Ohba, H. Yanai, H. Negishi, T. Mizutani, A. Takaoka, C. Taya, and T. Taniguchi. 2005. Spatiotemporal regulation of MyD88-IRF-7 signalling for robust type-I interferon induction. *Nature* 434: 1035–1040.
18. Shortman, K., and Y. J. Liu. 2002. Mouse and human dendritic cell subtypes. *Nat. Rev. Immunol.* 2: 151–161.
19. Asselin-Paturel, C., A. Boonstra, M. Dalod, I. Durand, N. Yessaad, C. Dezutter-Dambuyant, A. Vicari, A. O'Garra, C. Biron, F. Brière, and G. Trinchieri. 2001. Mouse type I IFN-producing cells are immature APCs with plasmacytoid morphology. *Nat. Immunol.* 2: 1144–1150.
20. Nakano, H., M. Yanagita, and M. D. Gunn. 2001. CD11c(+)B220(+)Gr-1(+) cells in mouse lymph nodes and spleen display characteristics of plasmacytoid dendritic cells. *J. Exp. Med.* 194: 1171–1178.
21. Björck, P. 2001. Isolation and characterization of plasmacytoid dendritic cells from Flt3 ligand and granulocyte-macrophage colony-stimulating factor-treated mice. *Blood* 98: 3520–3526.
22. Perussia, B., V. Fanning, and G. Trinchieri. 1985. A leukocyte subset bearing HLA-DR antigens is responsible for in vitro alpha interferon production in response to viruses. *Natural Immunity and Cell Growth Regulation* 4: 120–137.
23. Siegal, F. P., N. Kadowaki, M. Shodell, P. A. Fitzgerald-Bocarsly, K. Shah, S. Ho, S. Antonenko, and Y. J. Liu. 1999. The nature of the principal type 1 interferon-producing cells in human blood. *Science* 284: 1835–1837.
24. Kadowaki, N., S. Antonenko, and Y. J. Liu. 2001. Distinct CpG DNA and polyinosinic-polycytidylic acid double-stranded RNA, respectively, stimulate CD11c- type 2 dendritic cell precursors and CD11c+ dendritic cells to produce type I IFN. *J. Immunol.* 166: 2291–2295.
25. Lande, R., J. Gregorio, V. Facchinetti, B. Chatterjee, Y. H. Wang, B. Homey, W. Cao, Y. H. Wang, B. Su, F. O. Nestle, et al. 2007. Plasmacytoid dendritic cells sense self-DNA coupled with antimicrobial peptide. *Nature* 449: 564–569.
26. Yasuda, K., P. Yu, C. J. Kirschning, B. Schlatter, F. Schmitz, A. Heit, S. Bauer, H. Hochrein, and H. Wagner. 2005. Endosomal translocation of vertebrate DNA activates dendritic cells via TLR9-dependent and -independent pathways. *J. Immunol.* 174: 6129–6136.
27. Klinman, D. M. 2004. Immunotherapeutic uses of CpG oligodeoxynucleotides. *Nat. Rev. Immunol.* 4: 249–258.
28. Manegold, C., D. Gravenor, D. Woytowitz, J. Mezger, V. Hirsh, G. Albert, M. Al-Adhami, D. Readett, A. M. Krieg, and C. G. Leichman. 2008. Randomized phase II trial of a toll-like receptor 9 agonist oligodeoxynucleotide, PF-3512676, in combination with first-line taxane plus platinum chemotherapy for advanced-stage non-small-cell lung cancer. *J. Clin. Oncol.* 26: 3979–3986.
29. Fourcade, J., P. Kudela, P. A. Andrade Filho, B. Janjic, S. R. Land, C. Sander, A. Krieg, A. Donnenberg, H. Shen, J. M. Kirkwood, and H. M. Zarour. 2008. Immunization with analog peptide in combination with CpG and montanide expands tumor antigen-specific CD8+ T cells in melanoma patients. *J. Immunother.* 31: 781–791.
30. Seif, A. E., D. M. Barrett, M. Milone, V. I. Brown, S. A. Grupp, and G. S. Reid. 2009. Long-term protection from syngeneic acute lymphoblastic leukemia by CpG ODN-mediated stimulation of innate and adaptive immune responses. *Blood* 114: 2459–2466.
31. Lakadamyali, M., M. J. Rust, and X. Zhuang. 2006. Ligands for clathrin-mediated endocytosis are differentially sorted into distinct populations of early endosomes. *Cell* 124: 997–1009.
32. Bandholtz, L., Y. Guo, C. Palmberg, K. Mattsson, B. Ohlsson, A. High, J. Shabanowitz, D. F. Hunt, H. Jörnvall, H. Wigzell, et al. 2003. Hsp90 binds CpG oligonucleotides directly: implications for hsp90 as a missing link in CpG signaling and recognition. *Cell. Mol. Life Sci.* 60: 422–429.
33. Wagner, H. 2004. The immunobiology of the TLR9 subfamily. *Trends Immunol.* 25: 381–386.
34. Guiducci, C., G. Ott, J. H. Chan, E. Damon, C. Calacsan, T. Matray, K. D. Lee, R. L. Coffman, and F. J. Barrat. 2006. Properties regulating the nature of the plasmacytoid dendritic cell response to Toll-like receptor 9 activation. *J. Exp. Med.* 203: 1999–2008.
35. Rutz, M., J. Metzger, T. Gellert, P. Luppa, G. B. Lipford, H. Wagner, and S. Bauer. 2004. Toll-like receptor 9 binds single-stranded CpG-DNA in a sequence- and pH-dependent manner. *Eur. J. Immunol.* 34: 2541–2550.
36. Leadbetter, E. A., I. R. Rifkin, A. M. Hohlbaum, B. C. Beaudette, M. J. Shlomchik, and A. Marshak-Rothstein. 2002. Chromatin-IgG complexes activate B cells by dual engagement of IgM and Toll-like receptors. *Nature* 416: 603–607.
37. Boulé, M. W., C. Broughton, F. Mackay, S. Akira, A. Marshak-Rothstein, and I. R. Rifkin. 2004. Toll-like receptor 9-dependent and -independent dendritic cell activation by chromatin-immunoglobulin G complexes. *J. Exp. Med.* 199: 1631–1640.
38. Vallin, H., A. Perers, G. V. Alm, and L. Rönnblom. 1999. Anti-double-stranded DNA antibodies and immunostimulatory plasmid DNA in combination mimic the endogenous IFN-alpha inducer in systemic lupus erythematosus. *J. Immunol.* 163: 6306–6313.
39. Magnusson, M., S. Magnusson, H. Vallin, L. Rönnblom, and G. V. Alm. 2001. Importance of CpG dinucleotides in activation of natural IFN-alpha-producing cells by a lupus-related oligodeoxynucleotide. *Scand. J. Immunol.* 54: 543–550.
40. Minota, S., S. Koyasu, I. Yahara, and J. Winfield. 1988. Autoantibodies to the heat-shock protein hsp90 in systemic lupus erythematosus. *J. Clin. Invest.* 81: 106–109.
41. Conroy, S. E., G. B. Faulds, W. Williams, D. S. Latchman, and D. A. Isenberg. 1994. Detection of autoantibodies to the 90 kDa heat shock protein in systemic lupus erythematosus and other autoimmune diseases. *Br. J. Rheumatol.* 33: 923–926.
42. Twomey, B. M., V. B. Dhillon, S. McCallum, D. A. Isenberg, and D. S. Latchman. 1993. Elevated levels of the 90 kD heat shock protein in patients with systemic lupus erythematosus are dependent upon enhanced transcription of the hsp90 beta gene. *J. Autoimmun.* 6: 495–506.
43. Ripley, B. J., D. A. Isenberg, and D. S. Latchman. 2001. Elevated levels of the 90 kDa heat shock protein (hsp90) in SLE correlate with levels of IL-6 and autoantibodies to hsp90. *J. Autoimmun.* 17: 341–346.
44. Perdew, G. H., N. Hord, C. E. Hollenback, and M. J. Welsh. 1993. Localization and characterization of the 86- and 84-kDa heat shock proteins in Hepa 1c1c7 cells. *Exp. Cell Res.* 209: 350–356.
45. Akner, G., K. Mossberg, K. G. Sundqvist, J. A. Gustafsson, and A. C. Wikström. 1992. Evidence for reversible, non-microtubule and non-microfilament-dependent nuclear translocation of hsp90 after heat shock in human fibroblasts. *Eur. J. Cell Biol.* 58: 356–364.
46. Pisetsky, D. S., and A. M. Fairhurst. 2007. The origin of extracellular DNA during the clearance of dead and dying cells. *Autoimmunity* 40: 281–284.

Cancer Science
The official journal of the Japanese Cancer Association

Melanoma-targeted chemo-thermo-immuno (CTI)-therapy using *N*-propionyl-4-*S*-cysteaminylphenol-magnetite nanoparticles elicits CTL response via heat shock protein-peptide complex release

Akiko Sato,[1] Yasuaki Tamura,[2,6] Noriyuki Sato,[2] Toshiharu Yamashita,[1] Tomoaki Takada,[1] Makito Sato,[1] Yasue Osai,[1] Masae Okura,[1] Ichiro Ono,[1] Akira Ito,[3] Hiroyuki Honda,[4] Kazumasa Wakamatsu,[5] Shosuke Ito[5] and Kowichi Jimbow[1]

Departments of [1]Dermatology and [2]Pathology, Sapporo Medical University, Sapporo; [3]Department of Chemical Engineering, Faculty of Engineering, Kyusyu University, Fukuoka; [4]Department of Biotechnology, Nagoya University, Nagoya; [5]Department of Chemistry, Fujita Health University, Toyoake, Japan

(Received February 1, 2010/Revised April 22, 2010/Accepted May 4, 2010/Accepted manuscript online May 19, 2010/Article first published online June 28, 2010)

Melanogenesis substrate, *N*-propionyl-4-*S*-cysteaminylphenol (NPrCAP) is specifically taken up by melanoma cells and inhibits their growth by producing cytotxic free radicals. By taking advantage of this unique chemical agent, we have established melanoma-targeting intracellular hyperthermia by conjugating NPrCAP with magnetite nanoparticles (NPrCAP/M) upon exposure to an alternating magnetic field (AMF). This treatment causes cytotoxic reaction as well as heat shock responses, leading to elicitation of antitumor immune response, which was proved by tumor rechallenge test and CTL induction. We found the level of heat shock protein 72 (Hsp72) to be increased in the cell lysate and culture supernatant after intracellular hyperthermia. Melanoma-specific CD8$^+$ T-cell response to dendritic cells loaded with hyperthermia-treated tumor lysate was enhanced when compared with non-treated tumor lysate. When heat shock protein, particularly Hsp72, was immuno-depleted from hyperthermia-treated tumor cell lysate, specific CD8$^+$ T-cell response was abolished. Thus, it is suggested that antitumor immune response induced by hyperthermia using NPrCAP/M is derived from the release of HSP-peptide complex from degraded tumor cells. Therefore, this chemo-thermo-immuno (CTI)-therapy might be effective not only for primary melanoma but also for distant metastasis because of induction of systemic antimelanoma immune responses. (*Cancer Sci* 2010; 101: 1939–1946)

Melanoma has been increasing in incidence leading to a rise in morbidity and mortality in recent decades. Metastatic melanoma is extremely difficult to cure and continues to have a poor prognosis. Only 12% with metastatic melanoma survive for 5 years.[1] The reason for this poor prognosis is the lack of effective conventional therapies. Various types of therapies such as immunotherapy, chemotherapy, and biologic therapy have been studied in melanoma management. However, a very modest effect was recorded in advanced malignant melanoma. Therefore, there is an emerging need for innovative therapies for the control of advanced melanoma.

It has been reported that the intracellular hyperthermia using magnetic nanoparticles is effective for treating certain types of cancer in not only primary but also metastatic lesions.[2–8] Incorporated magnetic nanoparticles generate heat within the cells after exposure to the alternating magnetic field (AMF) due to hysteresis loss or relaxational loss.[9,10] One of us has shown that hyperthermic treatment using magnetite cationic liposomes (MCLs), which are cationic liposomes containing 10-nm magnetite nanoparticles, induces antitumor immunity by enhancement of heat shock protein (HSP) expression.[3,11–13] We previously proposed that cross-presentation of extracellular HSP-peptide complex released from hyperthermia-induced necrotic tumor cells is the mechanism for inducing antitumor immunity.[7] In this paper, we present evidence that tumor-derived HSP-peptide complex is responsible for the hyperthermia-mediated antitumor immunity.

In addition, exploitation of biological properties unique to melanoma cells may provide a novel approach to improve the effect of hyperthermic treatment. We have previously shown that the sulfur-amine analog of tyrosine, 4-S-cysteaminyl phenol (4-*S*-CAP), and its *N*-acetyl or propionyl derivatives (NAcCAP or NPrCAP) are good substrates for melanoma-specific targeting and therapy. They have been shown to cause selective cytotoxicity against melanocytes and melanoma cells after selective uptake. Therefore, they can be good candidates for developing antimelanoma chemotherapy because melanogenesis is inherently toxic and expressed uniquely in melanocytic cells.[14–17] Recently, we synthesized new magnetite nanoparticles, NPrCAP/M, on which NPrCAP was directly conjugated on the surface of magnetite nanoparticles.[18,19] We have shown that NPrCAP/M is specifically targeted to melanoma cells, and internalized and aggregated within their cell cytoplasm. In addition, we have observed that B16 melanoma cells, which were subjected to intracellular hyperthermia using NPrCAP/M with AMF exposure, were brought to necrotic cell death, resulting in tumor growth retardation.[18] Here we show that the intracellular hyperthermic treatment using NPrCAP/M with AMF exposure induces tumor-specific immune responses and therefore we call this antimelanoma therapy "chemo-thermo-immuno (CTI)" therapy. We demonstrate that CTI therapy-induced antimelanoma immunity is mediated through cross-presentation of up-regulated intracellular and extracellular HSPs-peptide complex derived from melanoma cells.

Materials and Methods

Mice and cells. Female C57BL/6 mice were obtained from Hokudo (Sapporo, Japan) and used at 4–6 weeks of age.

[6]To whom correspondence should be addressed.
E-mail: ytamura@sapmed.ac.jp

doi: 10.1111/j.1349-7006.2010.01623.x

B16-OVA is a B16F1 melanoma cells stably transfected with chicken ovalbumin (OVA) cDNA (kindly provided by Dr Y. Nishimura, Kumamoto University, Kumamoto, Japan). B16-OVA was cultured in DMEM supplemented 10% FCS and 250 μg/mL of hygromycin B. B3Z is a $CD8^+$ T-cell hybridoma that expresses LacZ in response to activation of T-cell receptors specific for the SIINFEKL peptide (SL8; OVA-immunodominant peptide) in the context of $H\text{-}2K^b$ (kindly provided by Dr N. Shastri, University of California, Berkeley, CA, USA). B16F1 melanoma cells, CT26 colon carcinoma cells, and LLC lung carcinoma cells were cultured in DMEM supplemented with 10% FCS. EL4 lymphoma cells, YAC-1 cells, and B3Z cells were cultured in complete RPMI supplemented with 10% FCS. Bone marrow-derived dendritic cells (DCs) were generated from the femurs and tibiae of C57BL/6 mice. The bone marrow was flushed out, and the leukocytes were obtained and cultured in complete RPMI-1640 with 10% FCS and 20 ng/mL GM-CSF (Endogen, Woburn, MA, USA) for 5 days. On day 3, fresh medium with GM-CSF was added to the plates for the day 5 cultures.

Preparation of NPrCAP/M. Magnetite nanoparticles (Fe_3O_4; average particle size, 10 nm) were kindly provided by Toda Kogyo (Hiroshima, Japan). The details of the preparation of NPrCAP/M are described elsewhere.[18] Briefly, magnetite nanoparticles were coated with aminosilane and conjugated with NPrCAP via maleimide cross-linkers. The resultant NPrCAP/M was suspended in 10 mL of H_2O. The degree of incorporation of NPrCAP to magnetite was 61.0 nmol/mg magnetite.

Antibodies. For depletion of HSPs from cell lysate, anti-Hsp72/Hsc73 mAb, anti-Hsp90α polyclonal antibody, anti-Hsp90 mAb, and anti-lysine-aspartic acid-glutamic acid-leucine (KDEL) mAb were used. Anti-Hsp72/Hsc73 mAb and anti-Hsp90mAb were used for western blotting. These antibodies were obtained from StressGen Biotechnologies Victoria, BC, Canada). Mouse IgG and Rabbit IgG were purchased from IBL (Takasaki, Japan).

Measurement of iron concentration in the NPrCAP/M-exposed cells. Subconfluently growing melanoma and non-melanoma cells ($8 \times 10^4/cm^2$) in a 25-cm^2 flask were re-fed with the medium containing 5.94 mg of NPrCAP/M or magnetite (84 mg/mL). To discriminate between incorporation of NPrCAP/M and magnetite by direct attachment to cells and that by diffusion from the medium, culture flasks were fixed on a slanted disc and rotated slowly for 30 min. After the cells were washed with PBS twice and collected, they were dissolved completely in 200 μL of concentrated HCl and incubated at 43°C for 30 min. Then, 10 mL of H_2O_2 and 4 mL of 1% potassium thiocyanate were added in sequence to the cell solution. The concentration of NPrCAP/M used in these experiments was 24.4 μM as NPrCAP.

Transplantation of tumor cells and intracellular hyperthermia. All of the animal experiments were conducted with the approval of the Animal Experiment Ethics Committee of Sapporo Medical University. B16-OVA cells (1×10^6) were subcutaneously transplanted into the right flank of C57BL/6 mice on day 0. NPrCAP/M nanoparticles (24.4 μM as NPrCAP, 100 μL) were injected subcutaneously into the tumor on days 7, 9, 11, and 13. A magnetic field was created using a horizontal coil (inner diameter, 7 cm; length, 7 cm) with a transistor inverter (LTG-100-05; Dai-ichi High Frequency, Tokyo, Japan).[4] The magnetic field frequency and intensity were 118 KHz and 30.6 KA/m (386 Oe), respectively. Twenty-four hours after injection, mice were subjected to AMF exposure to heat the tumor at 43°C for 30 min. The heated field was three dimensions, which was created using a horizontal coil with a transistor inverter. The mice whose tumors were injected with NPrCAP/M were put in a horizontal coil and exposed to AMF. Moreover, we monitored the temperature of the tumor surface as well as the rectal temperature using an optical fiber probe. The temperature of the tumor surface was maintained at 43°C and rectal temperature was about 38°C. Tumor growth was recorded once every 2 days. The cured mice were then rechallenged with a subcutaneous injection of B16-OVA cells (1×10^6) or irrelevant 3LL lung carcinoma cells (1×10^6) on the left flank. Tumor size was determined by the following formula: tumor volume = $0.5 \times (\text{length} \times \text{width}^2)$, where length and width were measured in millimeters.

Histopathology of tumor sections. Twenty-one days after tumor challenge, subcutaneous B16-OVA tumors were harvested and fixed in 10% formalin in PBS, then paraffin embedded and sectioned. Hematoxylin–eosin (H&E)-stained sections were prepared for analysis of therapeutic effect and gross infiltrate. For immunohistochemical analysis, the frozen tissues were stained with an antimouse CD4 mAb (Santa Cruz Biotechnology, Santa Cruz, CA, USA) or an antimouse CD8 mAb (Chemicon International, Temecula, CA, USA) and then incubated with HRP-conjugated goat antirat Ig (Dako, Tokyo, Japan), followed by hematoxylin counterstaining.

***In vitro* cytotoxicity assay.** After mice were treated by intracellular hyperthermia as described above, spleens were harvested on day 28, then 5×10^6 spleen cells were restimulated *in vitro* with irradiated B16-OVA cells in 2 mL of RPMI-1640 supplemented with 50 μM of β-mercaptethanol (Invitrogen, Carlsbad, CA, USA) and 10% FCS for 5 days. Cytotoxic activity of the effector cells against target cells (B16-OVA, EL4, EL4 loaded with SL8 peptide and YAC-1) was determined by standard ^{51}Cr release assay.

Quantification of HSPs. Cultured B16-OVA cells were exposed to NPrCAP/M for 30 min and irradiated by AMF to heat them at 43°C. After NPrCAP/M exposure with or without AMF irradiation, cells (1×10^6) were cultured in 1 mL of 10% RPMI for 72 h. Culture supernatant was collected at 12, 24, and 48 h, or cells escaping cell death were lysed at 72 h after intracellular hyperthermia by freezing and thawing and centrifugation at 2380 *g* for 5 min. The expression of Hsp72/Hsc73 and Hsp90 was determined by western blotting with an anti-Hsp72/Hsc73 mAb or anti-Hsp90 mAb. Heat shock protein (HSP) in the lysate or culture supernatant was quantified by the Hsp90α ELISA and Hsp70 ELISA kits (StressGen), which can detect and quantify Hsp90α and inducible Hsp72, respectively.

Cross-presentation of antigen derived from hyperthermia-treated tumor cell lysate by DCs. Cultured B16-OVA cells were exposed to NPrCAP/M for 30 min and irradiated by AMF to heat them at 43°C. After NPrCAP/M exposure with or without AMF irradiation, cells were cultured for 72 h and 1×10^7 of cells in 1 mL of 10% RPMI medium were lysed by three cycles of freezing and thawing and centrifugation at 2380*g* for 5 min. Dendritic cells DCs (1×10^5) derived from bone marrow of C57BL/6 mice were pulsed with the cell lysate (100 μL) and incubated with 1×10^5 B3Z T cell hybridoma. After overnight incubation, LacZ activity was measured by addition of 100 μL of chlorophenol red-β-D-galactopyranoside (CPRG, Roche, Basel, Switzerland) solution. The absorbance was measured at 595 nm after 4-h incubation at 37°C.

Immunodepletion of HSP. Cultured B16-OVA cells were treated and lysed as described above. The cell lysate (100 μL) was incubated with antibodies (5 μg each) against Hsp90, Hsp72/Hsc73, KDEL, or all of them. The mixture was added to 10 μL of protein A-Sepharose beads (50% slurry; GE Healthcare Japan, Tokyo, Japan), and the suspension was rotated at RT for 1 h. Then, the suspension was spun at 14 000*g* for 1 min. After removal of the beads, the supernatant was used for cross-presentation assay using B3Z as described above. Mouse IgG (15 μg) was used as an experimental control. Depletion was assessed by immunoblotting with anti-Hsp90, Hsp72/Hsc73, or KDEL antibodies.

doi: 10.1111/j.1349-7006.2010.01623.x

***In vivo* cross-presentation of antigen derived from melanoma cells after CTI therapy.** B16-OVA cells (1×10^6) were transplanted into the footpads of C57BL/6 mice on day 0. NPrCAP/M nanoparticles (24.4 μM as NPrCAP, 100 μL) were injected into the tumor on days 7, 9, 11, and 13. Twenty-four hours after injection, mice were subjected to AMF exposure to heat the tumor at 43°C for 30 min. Control mice were injected with PBS or NPrCAP/M nanoparticles alone without hyperthermia. After 5 h of the last CTI therapy against B16-OVA, popliteal nodes were removed and DCs were isolated using CD11c MACS beads (Miltenyi Biotec).Then, B3Z cells (1×10^5) were added to the DC culture (1×10^5) in 96-well flat-bottom plates and incubated at 37°C. Twenty-four hours after incubation, absorbance at 595 nm was measured.

Statistical analyses. All experiments were independently performed three times in triplicate. Comparisons between two groups were performed using Student's *t*-test. In the tumor transplantation assay, we determined statistical significance using Kruskal–Wallis one-way analysis. In all experiments, differences were considered statistically significant at $P < 0.05$.

Results

***N*-propionyl-4-*S*-cysteaminylphenol with magnetite nanoparticles (NPrCAP/M) was preferentially incorporated into melanoma cells.** To examine whether NPrCAP/M could be incorporated into melanoma cells more preferentially than magnetite alone, we compared amounts of iron molecules in cells after culture in the NPrCAP/M- or magnetite-containing media. As shown in Figure 1, B16F1, B16-OVA melanoma cells incorporated large amounts of iron derived from NPrCAP/M compared to that from magnetite alone. Non-melanoma CT26 colon carcinoma and LLC lung carcinoma cells captured a small amount of NPrCAP/M; however, the amount was not significantly different from that with magnetite alone or was almost the same as for magnetite. These data suggested that NPrCAP/M nanoparticle was an ideal agent for specific targeting to melanoma cells.

Antitumor effect of intracellular hyperthermia using NPrCAP/M with AMF exposure and its ability to induce antitumor immunity. We have recently reported the efficacy of melanoma growth inhibition by combination therapy of NPrCAP/M administration with AMF exposure.[19] B16F1 melanoma bearing mice treated with NPrCAP/M injection followed by hyperthermia showed apparent tumor growth retardation. In addition, we have observed that treatment with NPrCAP/M alone (without hyperthermia) also showed the growth suppression of B16F1 melanoma, indicating that NPrCAP/M has a chemotherapeutic effect. In this paper, we used B16-OVA, which was B16 melanoma transfected with OVA as a surrogate tumor antigen, to examine the antigen-specific antitumor immune response. Mice were transplanted with B16-OVA melanoma cells and treated with NPrCAP/M injection followed by hyperthermia or NPrCAP/M injection alone as described in the Materials and Methods. Histopathological examination of the day 21 tumors without treatment showed that inflammatory infiltrates were poorly detected including $CD8^+$ T cells and $CD4^+$ T cells (Fig. 2a-i, -ii, -iii, -iv). In contrast, treatment with combination of NPrCAP/M injection and hyperthermia induced apparent tumor destruction and necrosis with deposit of NPrCAP/M particles (Fig. 2a-v, -vi). In addition, a dense inflammatory infiltrate including neutrophiles, macrophages, plasma cells, and lymphocytes was observed around the residual tumor cells (Fig. 2a-vii, -viii). Furthermore, we have observed that this infiltrate included both $CD8^+$ T cells and $CD4^+$ T cells (Fig. 2a-ix, -x). These T cells were hardly seen around the tumor without treatment or with NPrCAP/M without AMF exposure (data not shown). Tumor volume in the group treated by combination of NPrCAP/M injection and hyperthermia was significantly reduced compared with the non-treated control group ($P = 0.0025$) and the group of NPrCAP alone ($P = 0.023$) (Fig. 2b). Six out of 10 mice in the group treated by NPrCAP/M injection and hyperthermia were cured. In contrast, all mice died of tumor burden in the treatment with NPrCAP/M without AMF and control groups. Interestingly, both NPrCAP/M with and without AMF exposure resulted in a significant and equal reduction of melanoma tumor volume by 17 days after tumor challenge. However, the tumors of mice treated with NPrCAP/M without AMF exposure grew rapidly after day 17. This suggested that hyperthermia might be required for the complete elimination of melanoma tumors. To examine whether cured mice developed antitumor immune responses, these mice were rechallenged with live B16-OVA melanoma cells or irrelevant mouse lung carcinoma LLC 4 weeks after NPrCAP/M and hyperthermic treatment. As a result, all cured mice rejected a rechallenge of live B16-OVA melanoma cells, but not LLC lung carcinoma cells (Fig. 2c). These data indicated that intracellular hyperthermia using NPrCAP/M with AMF exposure induced specific antitumor immunity.

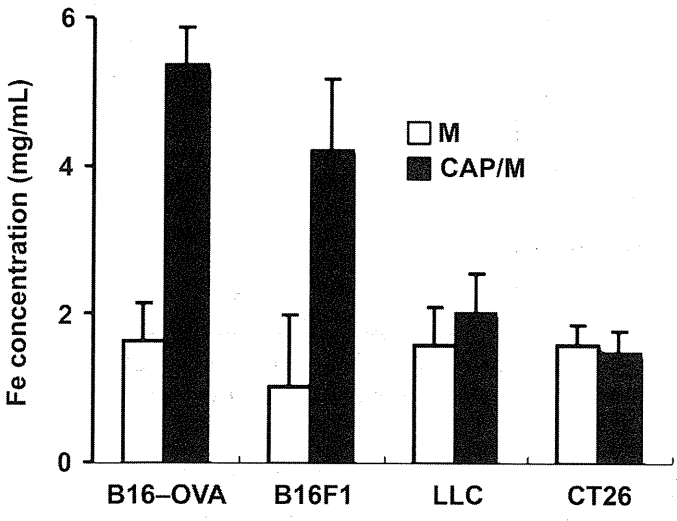

Fig. 1. *N*-propionyl-4-*S*-cysteaminylphenol with magnetite nanoparticles (NPrCAP/M) was preferentially incorporated into melanoma cells. Subconfluently growing melanoma and non-melanoma cells ($8 \times 104/cm^2$) in a 25 cm^2 flask were fed with medium containing 5.94 mg of NPrCAP/M or magnetite (84 mg/mL) for 30 min. Iron concentration of magnetite nanoparticles was measured using the potassium thiocyanate method.

Induction of tumor-specific CTL by intracellular hyperthermia. To analyze the mechanism for the generation of antitumor immunity by NPrCAP/M and hyperthermia, we examined CTL induction in mice after intracellular hyperthermia. Spleen cells of mice after hyperthermia showed high cytotoxicity against B16-OVA melanoma cells compared to EL4 lymphoma and YAC-1 cells. In addition, spleen cells also showed high cytotoxicity against EL4 pulsed with SL8 peptide derived from OVA protein (Fig. 3). These results suggest that intracellular hyperthermia using NPrCAP/M can elicit specific tumor immunity by inducing CTL against B16-OVA melanoma cells.

Enhanced expression of Hsp72 in B16-OVA melanoma cell after intracellular hyperthermia. We examined the expression of HSPs in tumor cells treated with NPrCAP with AMF exposure *in vitro* by western blotting and ELISA. The protein level of Hsp72 but not Hsc73 or Hsp90 was increased at 48 h after hyperthermia (Fig. 4a). Similarly, the concentration of Hsp72 in cell lysate resulted in a three-fold increase at 72 h after hyperthermia, compared to cells without treatment (Fig. 4b). However, the concentration of Hsp90 did not change (Fig. 4c).

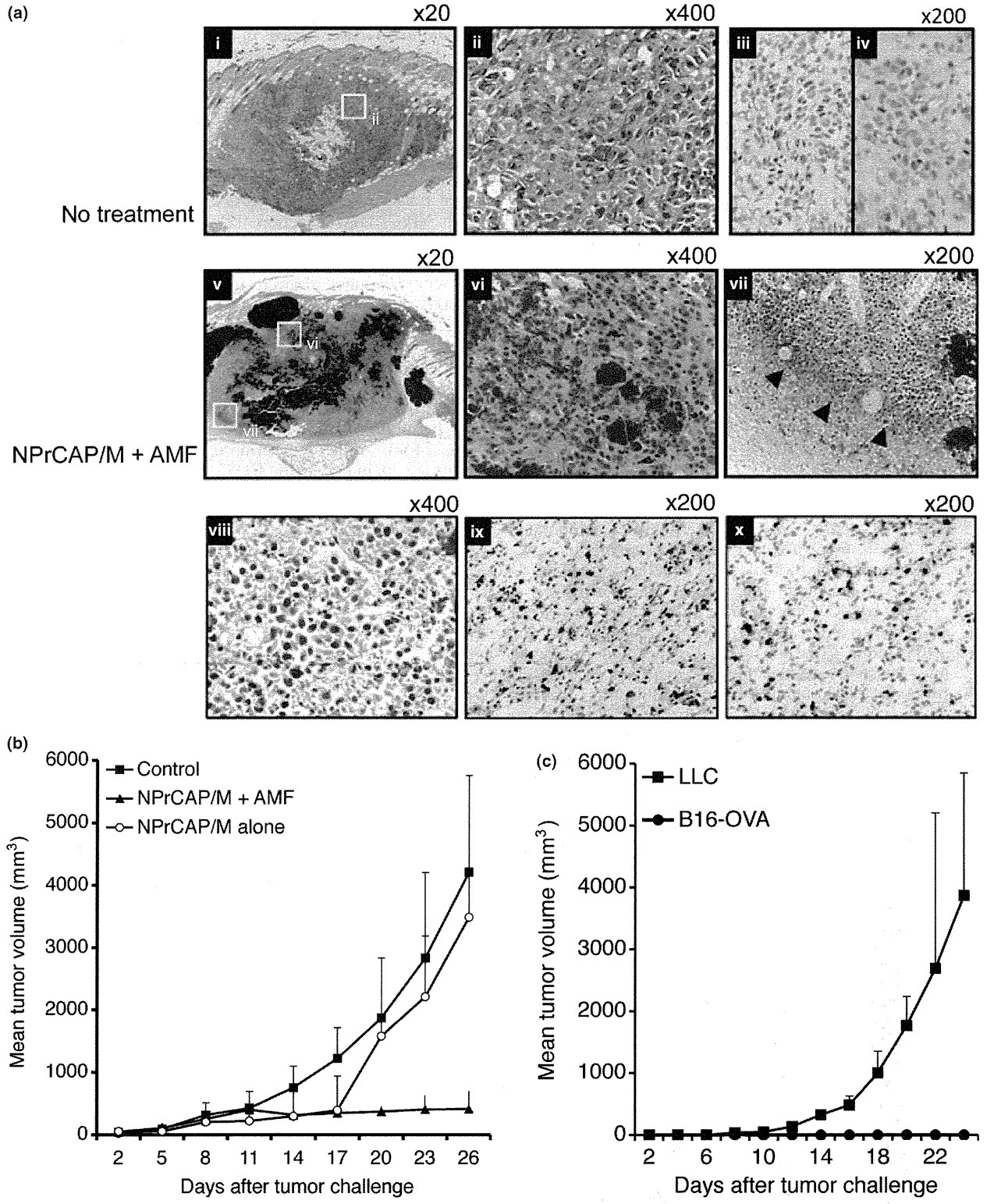

Fig. 2. Antitumor effect and tumor-specific immunity induced by intracellular hyperthermia using *N*-propionyl-4-*S*-cysteaminylphenol with magnetite nanoparticles (NPrCAP/M) and alternating magnetic field (AMF) exposure. (a) Pre-established subcutaneous B16-OVA tumors without treatment (i,ii,iii,iv) or intracellular hyperthermia using NPrCAP/M with AMF exposure (v,vi,vii,viii,ix,x) were harvested and analyzed histologically using H&E-stained sections. Intracellular hyperthermia using NPrCAP with AMF exposure induced tumor destruction and inflammatory infiltrate (arrow head). The frozen tissues excised from mice untreated or treated with NPrCAP/M with AMF exposure were stained with an antimouse CD8 mAb (iii,ix) or CD4 mAb (iv,x). (b) Tumor growth of B16-OVA melanoma cells in non-treated control mice (n = 10), mice treated with NPrCAP/M with AMF exposure (n = 10), or mice treated with NPrCAP/M alone (n = 10). Points, mean tumor volume (mm^3); bars, SD. (c) The development of tumor specific immunity by intracellular hyperthermia. Mice cured by intracellular hyperthermia were rechallenged with B16-OVA melanoma cells (n = 3) or lung carcinoma LLC (n = 3). Mice were transplanted with 1×10^6 B16-OVA cells and then the tumor growth rates of each group were compared using the average tumor size. Points, mean tumor volume (mm^3); bars, SD. Results shown are representative of three different experiments.

doi: 10.1111/j.1349-7006.2010.01623.x

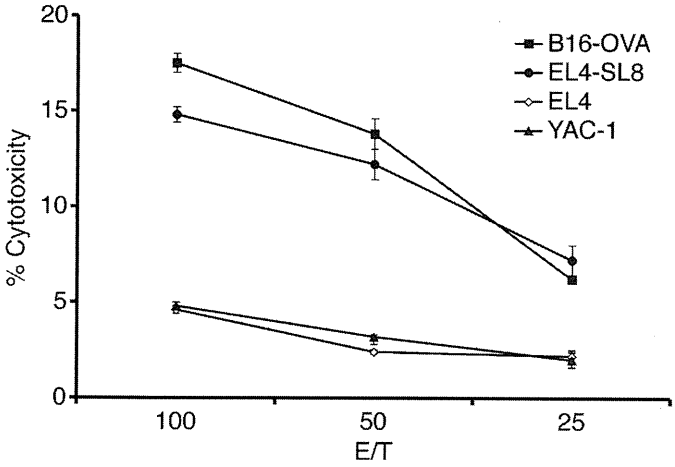

Fig. 3. Induction of tumor-specific CTL by intracellular hyperthermia. Analysis of spelenocytes cytotoxic activity against B16-OVA melanoma cells, EL4, EL4 pulsed with SL8 peptide, and YAC-1 in ^{51}Cr release assay. Mice were treated by *N*-propionyl-4-*S*-cysteaminylphenol with magnetite nanoparticles (NPrCAP/M) injection followed by alternating magnetic field (AMF) exposure. Four weeks after treatment, spleen cells were removed and stimulated with irradiated B16-OVA cells. Cytotoxic activity of spleen cells against B16-OVA cells, EL4 cells, EL4 cells pulsed with SL8 peptide, or YAC-1 cells was determined by standard ^{51}Cr-release assay. Bars, SD.

Treatment with NPrCAP alone decreased the level of intracellular Hsp72 and Hsp90. We are currently investigating the underlying mechanism. From the results obtained, we hypothesized that hyperthermia using NPrCAP/M might induce tumor immunity through up-regulation of Hsp72.

Intracellular hyperthermia using NPrCAP/M with AMF exposure results in the release of HSPs into the extracellular milieu. It has been demonstrated that once cancer cells become necrotic, several HSPs, above all, Hsp72 and Hsp90, are released from cells and might act as a danger signal, subsequently eliciting cell-specific immune responses. We therefore examined whether Hsp72 and Hsp90 would be released from necrotic melanoma cells after intracellular hyperthermia *in vitro*. Culture supernatants from B16-OVA were collected at 12, 24, and 48 h after intracellular hyperthermia and the quantity of Hsp72 and Hsp90 was evaluated using ELISA. Although Hsp72 and Hsp90 were detected at 48 h after hyperthermia, concentration of extracellular Hsp72 was a 4.5-fold higher than that of Hsp90 (Fig. 4d). These *in vitro* results suggested that treatment of B16-OVA melanoma with intracellular hyperthermia would release HSPs, in particular Hsp72, into extracellular milieu *in vivo* and these extracellular HSPs might play an important role in inducing antitumor immunity.

$CD8^+$ T-cell response against DCs loaded with B16-OVA melanoma cell lysate after intracellular hyperthermia. To analyze the mechanism of tumor specific CTL induction, we examined B3Z $CD8^+$ T-cell response against DCs loaded with supernatant from B16-OVA culture after intracellular hyperthermia. However, only a very modest response was observed (data not shown). One of the reasons for this modest response may be the degradation of peptide chaperoned by HSPs by protease in the culture medium. We therefore decided to use melanoma cell lysate after hyperthermia. NPrCAP/M loaded B16-OVA melanoma cells were subjected to AMF irradiation and cultured for 72 h. Melanoma cells were lysed by three cycles of freezing and thawing. Dendritic cells (DCs) derived from mouse bone marrow were loaded with the lysate for 2 h and then cultured with B3Z $CD8^+$ T-cell hybridoma. B3Z response against DC loaded with B16-OVA melanoma cell lysate increased after intracellular hyperthermia using NPrCAP/M, compared with non-heated cells and cells loaded NPrCAP/M without AMF exposure (Fig. 5a). These data demonstrated that loading DCs with lysate derived from melanoma cells treated with hyperthermia enhanced the cross-presentation of B16-OVA-specific antigen peptide.

Effects of immunodepletion of HSPs on $CD8^+$ T-cell response. Next, we investigated the underlying mechanism

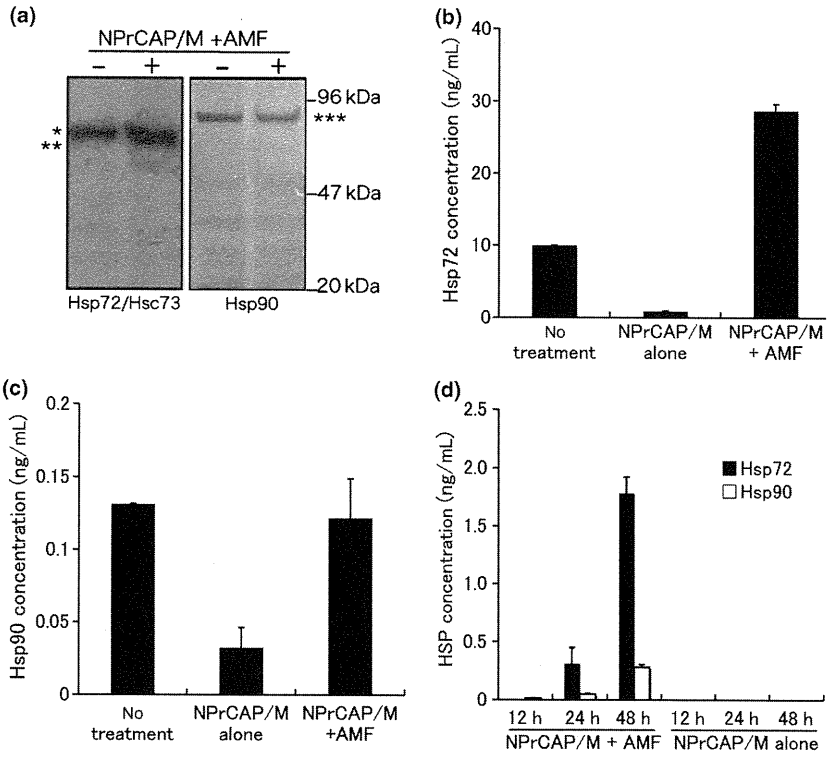

Fig. 4. Heat shock protein (HSP) expression in tumor cells after intracellular hyperthermia. (a–c) B16-OVA cells were subjected to hyperthermia using *N*-propionyl-4-*S*-cysteaminylphenol with magnetite nanoparticles (NPrCAP/M) with alternating magnetic field (AMF) exposure *in vitro*. Seventy-two hours after intracellular hyperthermia (+) or left untreated (–), the expression of Hsp72 and Hsp90 was determined by western blotting with an anti-Hsp72/Hsc73 mAb or anti-Hsp90 mAb (a). *Hsc73, **Hsp72, ***Hsp90. The expression of Hsp72 was markedly enhanced by intracellular hyperthermia. Heat shock protein (HSP) in the lysate was quantified by the Hsp72 ELISA (b) and Hsp90 ELISA kits (c). (d) Hsp72 and Hsp90 in the 12-, 24- and 48-h culture supernatant after intracellular hyperthermia were measured using ELISA. Bars, SD. Results shown are representative of three different experiments.

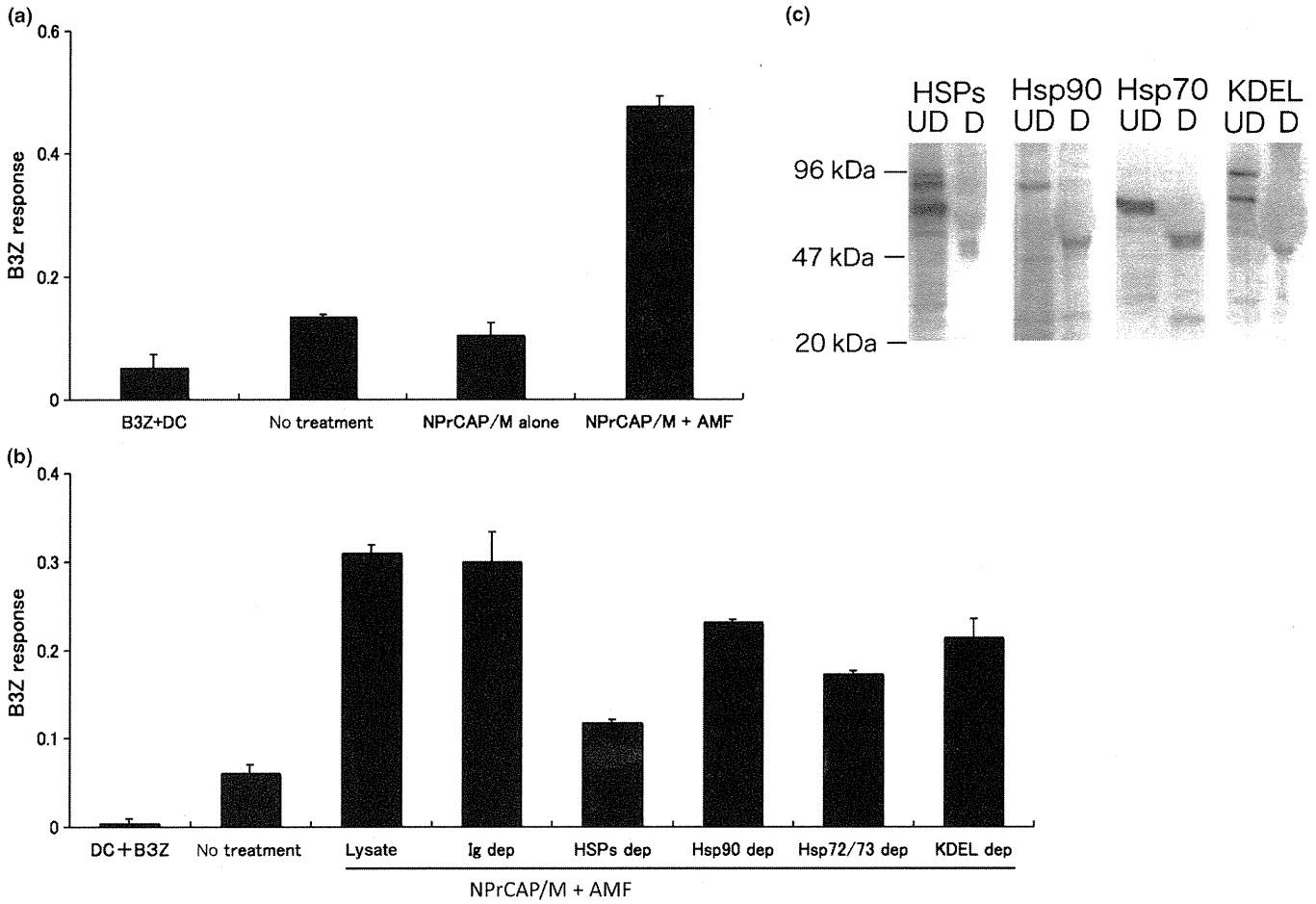

Fig. 5. $CD8^+$ T-cell response against dendritic cells (DCs) pulsed with B16-OVA melanoma cell lysate after intracellular hyperthermia and effect of heat shock protein (HSP) depletion. (a) B16-OVA cells were subjected to *N*-propionyl-4-*S*-cysteaminylphenol with magnetite nanoparticles (NPrCAP/M) exposure and alternating magnetic field (AMF) irradiation, then lysed by freezing and thawing. Dendritic cells (DCs) were pulsed with the cell lysate, and cultured overnight with B3Z and the absorbance of β-galactosidase activity was measured at 595 nm. Bars, SD. (b) Lysates of the cells were immunoprecipitated with anti-Hsp72/Hsc73 antibody, anti-Hsp90 antibody and anti-KDEL antibody. Immunoprecipitates were removed from lysate. After being pulsed with the HSP-depleted lysate, DCs were incubated with B3Z T cell hybridoma and the absorbance of β -galactosidase activity was measured at 595 nm. Bars, SD. (c) Cell lysates were depleted of HSPs (above lanes) with antibodies specific for each HSP. Immunoblots were of depleted (D) or undepleted (UD) lysates. Results shown are representative of five different experiments.

responsible for the enhancement of cross-presentation by intracellular hyperthermia. Hyperthermia has long been shown to induce the expression of HSPs within tumor cells, which have been shown to chaperone tumor-associated antigen peptides. To investigate the role of HSPs in intracellular hyperthermia-induced $CD8^+$ T-cell response, we depleted HSPs from lysate using anti-HSP antibody, and measured $CD8^+$ T-cell response against DCs loaded with the HSP-depleted lysate. Depletion of major HSPs (Hsp72/Hsc73, Hsp90, and ER-resident HSPs) from NPrCAP/M and hyperthermic treated B16-OVA cell lysate caused a loss of 59% of initial B3Z response ($P = 0.0001$ *vs* depletion with control Ig) (Fig. 5b), whereas depletion with control Ig did not show any effect. Importantly, depletion of Hsp72/Hsc73 exhibited a 44% reduction of activity and it was best decreased in response in the HSP depletion assay. The inhibition rate was statistically significant compared with the depletion with control Ig ($P = 0.001$). Depletion of Hsp90 or ER resident HSPs caused a loss of 25% ($P = 0.0857$) or 31% ($P = 0.0034$) of the initial activity, respectively. Immunoblots showed that depletion of each HSP was complete (Fig. 5c). These results suggested that Hsp72/Hsc73, Hsp90, and ER-resident HSPs were involved in the induction of CTL response at various extents. In addition, our data demonstrated that these HSPs chaperoned antigenic peptides and extracellular HSP-peptide complexes were cross-presented by DCs, followed by specific CTL activation. Notably, Hsp72/Hsc73 was largely responsible for the observed T-cell response. As shown in Figure 4, these data were consistent with the enhanced expression of Hsp72 within the melanoma cells. Thus, DCs loaded with intracellular hyperthermia-treated melanoma cell lysate are more efficient than DCs loaded with untreated melanoma cell lysate in cross-presentation to CTLs.

Dendritic cells (DCs) derived from tumor-draining lymph nodes cross-present melanoma-associated antigen after CTI therapy. We examined whether melanoma-associated antigen was indeed cross-presented by DCs within tumor-draining lymph nodes after CTI therapy. To test this, we transplanted B16 melanoma cells into the footpads of mice. After three rounds of CTI therapy, tumor-draining popliteal nodes were removed and DCs were isolated and cultured with B3Z. B3Z response against regional lymph node-derived DCs of CTI-treated mice was evident when compared to PBS control or NPr-CAP/M injection without hyperthermia (Fig. 6). We therefore conclude that intracellular hyperthermia using NPrCAP/M with

doi: 10.1111/j.1349-7006.2010.01623.x

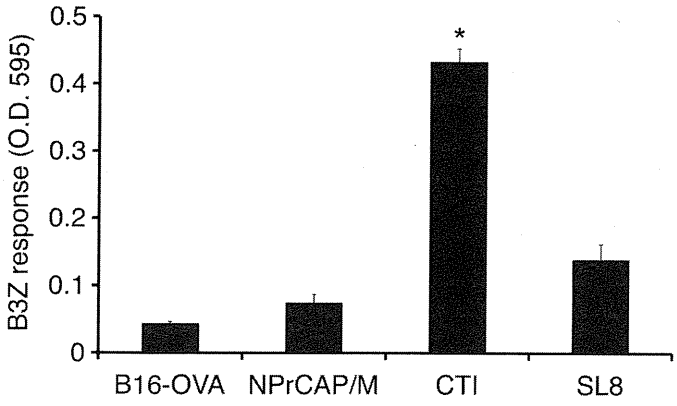

Fig. 6. Dendritic cells (DCs) derived from tumor-draining lymph nodes cross-present melanoma-associated antigen after CTI therapy. B16-OVA cells (1×10^6) were transplanted into the footpads of C57BL/6 mice on day 0. *N*-propionyl-4-*S*-cysteaminylphenol with magnetite nanoparticles (NPrCAP/M) nanoparticles (24.4 mM as NPrCAP, 100 mL) were injected into the tumor on days 7, 9, 11, and 13. Twenty-four hours after injection, mice were subjected to alternating magnetic field (AMF) exposure to heat the tumor at 43°C for 30 min. Control mice were injected with PBS or NPrCAP/M nanoparticles alone without hyperthermia. After 5 h of the last CTI therapy against B16-OVA, tumor-draining popliteal nodes were removed and DCs were isolated, then cultured with B3Z cells. Twenty-four hours after incubation, absorbance at 595 nm was measured. Bars, SD. $*P < 0.01$; paired Student's *t*-test. Data are representative of three independent experiments.

AMF exposure promotes OVA-derived peptide presentation on DCs both *in vitro* and *in vivo*.

Discussion

In this study, we showed that intracellular hyperthermia of melanoma cells using NPrCAP/M with AMF exposure elicited antitumor immune responses via cross-presentation of HSP-chaperoned antigen. Moreover, we demonstrated that DCs derived from tumor-draining lymph nodes indeed cross-presented melanoma-associated antigen after CTI therapy. It has been believed that enhanced expression of intracellular HSPs by hyperthermia plays an important role in the induction of antitumor immunity.[11,20] Moreover, it has been demonstrated that overexpression of HSPs, particularly Hsp72, causes increased tumor immunogenicity due to augmentation of the chaperoning ability of antigenic peptide, thereby augmenting the presentation of antigenic peptide in the context of MHC class I molecules.[21,22] However, in order to prime tumor-specific immunity, it is necessary to present tumor antigen in the context of MHC class I in conjunction with the co-stimulation signal through co-stimulatory molecules such as B7.1 and B7.2 by professional antigen-presenting cells such as DCs. Dendritic cells (DCs) have the unique capacity to take up, process, and present exogenous antigens in association with MHC class I molecules. This process is termed cross-presentation and the resulting $CD8^+$ T-cell priming is referred to as cross-priming. It has been demonstrated that some exogenous antigens such as HSPs[23–27] and particulate protein antigens[28] gain access to the MHC class I processing pathway and initiate CTL responses. This exogenous pathway is important for the development of $CD8^+$ CTL responses against tumors and infectious pathogens that do not have access to the classical MHC class I pathway.

Here, we showed that the HSPs-antigen peptide complex released from melanoma cells treated with intracellular hyperthermia is taken up by DCs and cross-presented HSP-chaperoned peptide in the context of MHC class I molecules (Fig. 7). Our CTI therapy induced NPrCAP- as well as heat-mediated melanoma cell necrosis to NPrCAP/M incorporated cells. We have reported that repeated hyperthermia (three cycles of NPrCAP/M injection and AMF irradiation) was required to induce the maximal antitumor immune responses.[19] If melanoma cells escape from necrotic cell death, repeated hyperthermia should produce necrotic cell death of previously heat shocked-melanoma cells in which HSPs were induced. In fact, our data suggested that Hsp72/Hsc73, Hsp90, and ER-resident

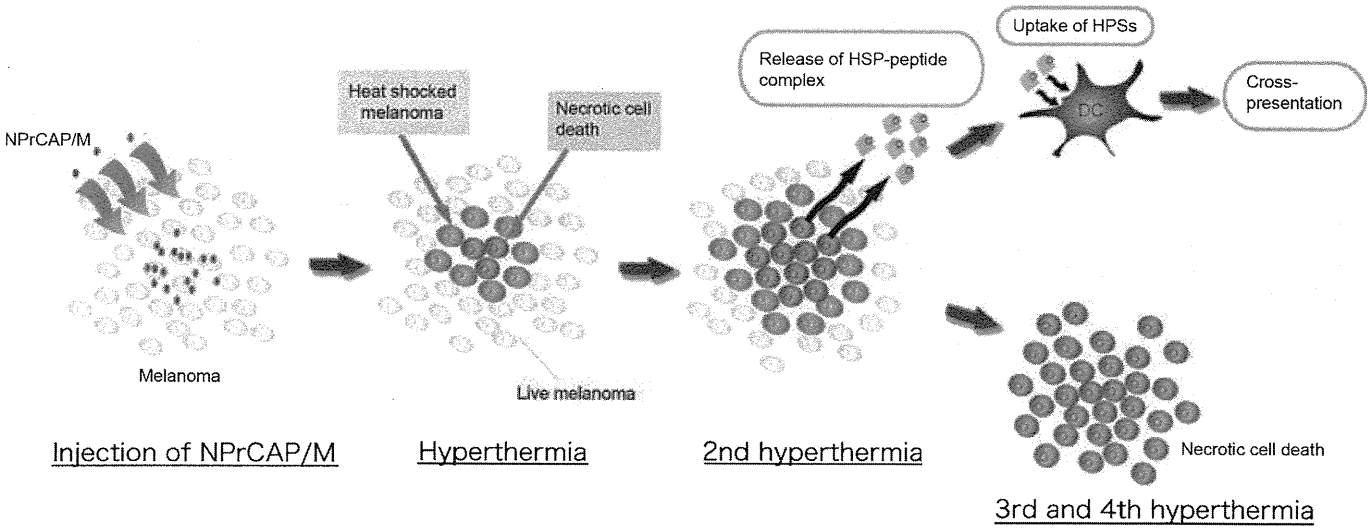

Fig. 7. Schema of intracellular hyperthermia using *N*-propionyl-4-*S*-cysteaminylphenol with magnetite nanoparticles (NPrCAP/M) with alternating magnetic field (AMF) exposure. Injected NPrCAP/M nanoparticles are specifically incorporated in melanoma cells. Intracellular hyperthermia can induce necrotic cell death and adjacent live melanoma cells suffer heat shock, resulting in increased level of intracellular heat shock protein (HSP)-peptide complexes. Repeated hyperthermia turns heat-shocked cells to necrotic cells, leading to the release of their intracellular contents, including HSPs-peptide complexes, into extracellular milieu. The released HSPs-peptide complexes are taken up by dendritic cells (DCs). Then, DCs migrate into regional lymph nodes and cross-present HSP-chaperoned antigenic peptides to $CD8^+$ T cells in the context of MHC class I molecules, thereby inducing antimelanoma CTLs. Finally, the remaining melanoma cells are killed by repeated hyperthermia or by the melanoma-specific CTLs.

HSPs participated in the induction of $CD8^+$ T-cell response. In particular, among HSPs, Hsp72 was largely responsible for the augmented antigen presentation to $CD8^+$ T cells. As Hsp72 is known to up-regulate in response to hyperthermia or heat shock treatment,[11] newly synthesized Hsp72 has a chance to bind to the heat-denatured melanoma-associated antigen.

Taken together, intracellular hyperthermia using NPrCAP/M is a promising treatment for improvement of clinical effects, especially for patients with advanced metastatic melanomas, and even for prevention of recurrence and/or metastasis for early melanomas because of induction of systemic antimelanoma immunity.

Acknowledgments

We thank Dr Shastri for providing B3Z T cell hybridoma, Dr Nishimura for providing B16-OVA, and Toda Kogyo Co. for providing the magnetite. This work was supported by a Health and Labor Sciences Research Grant-in-Aid for Research on Advanced Medical Technology from the Ministry of Health, Labor and Welfare of Japan.

Disclosure Statement

The authors have no conflict of interest.

References

1 Balch CM, Buzaid AC, Soong SJ *et al.* Final version of the American Joint Committee on Cancer staging system for cutaneous melanoma. *J Clin Oncol* 2001; **19**: 3635–48.
2 Yanase M, Shinkai M, Honda H, Wakabayashi T, Yoshida J, Kobayashi T. Intracellular hyperthermia for cancer using magnetite cationic liposomes: an in vivo study. *Jpn J Cancer Res* 1998; **89**: 463–9.
3 Kawai N, Ito A, Nakahara Y *et al.* Anticancer effect of hyperthermia on prostate cancer mediated by magnetite cationic liposomes and immune-response induction in transplanted syngeneic rats. *Prostate* 2005; **64**: 373–81.
4 Ito A, Shinkai M, Honda H, Kobayashi T. Medical application of functionalized magnetic nanoparticles. *J Biosci Bioeng* 2005; **100**: 1–11.
5 Yanase M, Shinkai M, Honda H, Wakabayashi T, Yoshida J, Kobayashi T. Antitumor immunity induction by intracellular hyperthermia using magnetite cationic liposomes. *Jpn J Cancer Res* 1998; **89**: 775–82.
6 Ito A, Shinkai M, Honda H, Wakabayashi T, Yoshida J, Kobayashi T. Augmentation of MHC class I antigen presentation via heat shock protein expression by hyperthermia. *Cancer Immunol Immunother* 2001; **50**: 515–22.
7 Ito A, Kobayashi T, Honda H. A mechanism of antitumor immunity induced by hyperthermia. *Jpn J Hyperthermic Oncol* 2005; **21**: 1–19.
8 Ito A, Takeshi K. Intracellular hyperthermia using magnetite nanoparticles: a novel method for hyperthermia clinical applications. *Thermal Medicine* 2008; **24**: 113–29.
9 Shinkai M, Yanase M, Honda H, Wakabayashi T, Yoshida J, Kobayashi T. Intracellular hyperthermia for cancer using magnetite cationic liposomes: in vitro study. *Jpn J Cancer Res* 1996; **87**: 1179–83.
10 Hergt R, Dutz S, Mueller R, Zeisberger M. Magnetite particle hyperthermia: nanoparticle magnetism and materials development for cancer therapy. *J Phys Condens Matter* 2006; **18**: S2919–34.
11 Ito A, Shinkai M, Honda H *et al.* Heat shock protein 70 expression induces antitumor immunity during intracellular hyperthermia using magnetite nanoparticles. *Cancer Immunol Immunother* 2003; **52**: 80–8.
12 Ito A, Matsuoka F, Honda H, Kobayashi T. Antitumor effects of combined therapy of recombinant heat shock protein 70 and hyperthermia using magnetic nanoparticles in an experimental subcutaneous murine melanoma. *Cancer Immunol Immunother* 2004; **53**: 26–32.
13 Ito A, Honda H, Kobayashi T. Cancer immunotherapy based on intracellular hyperthermia using magnetite nanoparticles: a novel concept of "heat-controlled necrosis" with heat shock protein expression. *Cancer Immunol Immunother* 2006; **55**: 320–8.
14 Ito Y, Jimbow K. Selective cytotoxicity of 4-S-cysteaminylphenol on follicular melanocytes of the black mouse: rational basis for its application to melanoma chemotherapy. *Cancer Res* 1987; **47**: 3278–84.
15 Miura S, Ueda T, Jimbow K, Ito S, Fujita K. Synthesis of cysteinylphenol, cysteaminylphenol, and related compounds, and in vivo evaluation of antimelanoma effect. *Arch Dermatol Res* 1987; **279**: 219–25.
16 Miura T, Jimbow K, Ito S. The in vivo antimelanoma effect of 4-S-cysteaminylphenol and its n-acetyl derivative. *Int J Cancer* 1990; **46**: 931–4.
17 Thomas PD, Kishi H, Cao H *et al.* Selective incorporation and specific cytocidal effect as the cellular basis for the antimelanoma action of sulphur containing tyrosine analogs. *J Invest Dermatol* 1999; **113**: 928–34.
18 Sato M, Yamashita T, Ohkura M *et al.* N-propionyl- cysteaminylphenol - magnetite conjugate (NPrCAP/M) is a nanoparticle for the targeted growth suppression of melanoma cells. *J Invest Dermatol* 2009; **129**: 2233–41.
19 Takada T, Yamashita T, Sato M *et al.* Growth inhibition of re-challenge B16 melanoma transplant by conjugates of melanogenesis substrate and magnetite nanoparticles as the basis for developing melanoma-targeted chemo-thermo-immunotherapy. *J Biomed Biotechnol* 2009; **2009**: 457936.
20 Mise K, Kan N, Okino T *et al.* Effect of heat treatment on tumor cells and antitumor effector cells. *Cancer Res* 1990; **50**: 6199–202.
21 Wells AD, Rai SK, Salvato MS, Band H, Malkovsky M. Hsp72-mediated augmentation of MHC class I surface expression and endogenous antigen presentation. *Int Immunol* 1998; **10**: 609–17.
22 Ito A, Matsuoka F, Honda H, Kobayashi T. Heat shock protein 70 gene therapy combined with hyperthermia using magnetic nanoparticles. *Cancer Gene Ther* 2003; **10**: 918–25.
23 Udono H, Srivastava PK. Comparison of tumor-specific immunogenicities of stress-induced proteins gp96, hsp90, and hsp70. *J Immunol* 1994; **152**: 5398–403.
24 Tamura Y, Peng P, Liu K, Daou M, Srivastava PK. Immunotherapy of tumors with autologous tumor-derived heat shock protein preparations. *Science* 1997; **278**: 117–20.
25 Moroi Y, Mayhew M, Trcka J *et al.* Induction of cellular immunity by immunization with novel hybrid peptides complexed to heat shock protein 70. *Proc Natl Acad Sci USA* 2000; **97**: 3485–90.
26 Kurotaki T, Tamura Y, Ueda G *et al.* Efficient Cross-Presentation by Heat Shock Protein 90-Peptide Complex-Loaded Dendritic Cells via an Endosomal Pathway. *J Immunol* 2007; **179**: 1803–13.
27 Kutomi G, Tamura Y, Okuya K *et al.* Targeting to static endosome is required for efficient cross-presentation of endoplasmic reticulum-resident oxygen-regulated protein 150-peptide complexes. *J Immunol* 2009; **183**: 5861–9.
28 Shen L, Sigal LJ, Boes M, Rock KL. Important role of cathepsin S in generating peptides for TAP-independent MHC class I crosspresentation in vivo. *Immunity* 2004; **21**: 155–65.

doi: 10.1111/j.1349-7006.2010.01623.x